This is a repository copy of *Evaluation of multiaxial high-cycle fatigue criteria under proportional loading for S355 steel*.

White Rose Research Online URL for this paper:
https://eprints.whiterose.ac.uk/167455/

Version: Accepted Version

Article:

Dantas, R., Correia, J., Lesiuk, G. et al. (5 more authors) (2021) Evaluation of multiaxial high-cycle fatigue criteria under proportional loading for S355 steel. Engineering Failure Analysis, 120. 105037. ISSN 1350-6307

https://doi.org/10.1016/j.engfailanal.2020.105037

Article available under the terms of the CC-BY-NC-ND licence (https://creativecommons.org/licenses/by-nc-nd/4.0/).

Reuse

This article is distributed under the terms of the Creative Commons Attribution-NonCommercial-NoDerivs (CC BY-NC-ND) licence. This licence only allows you to download this work and share it with others as long as you credit the authors, but you can't change the article in any way or use it commercially. More information and the full terms of the licence here: https://creativecommons.org/licenses/

Takedown

If you consider content in White Rose Research Online to be in breach of UK law, please notify us by emailing eprints@whiterose.ac.uk including the URL of the record and the reason for the withdrawal request.

eprints@whiterose.ac.uk
https://eprints.whiterose.ac.uk/

EVALUATION OF MULTIAXIAL HIGH-CYCLE FATIGUE CRITERIA UNDER PROPORTIONAL LOADING FOR S355 STEEL

Rita Dantas[a],*, José Correia[a],*, Grzegorz Lesiuk[b], Dariusz Rozumek[c], Shun-Peng Zhu[d], Abílio de Jesus[a], Luca Susmel[e] and Filippo Berto[f]

[a] INEGI & CONSTRUCT, Faculty of Engineering, University of Porto, Rua Dr. Roberto Frias, 4200-465 Porto, Portugal.

[b] Faculty of Mechanical Engineering, Department of Mechanics, Materials Science and Engineering, Wrocław University of Science and Technology, Smoluchowskiego 25, 50-370 Wrocław, Poland.

[c] Opole University of Technology, Department of Mechanics and Machine Design, Mikołajczyka 5, 45-271 Opole, Poland.

[d] School of Mechanical and Electrical Engineering, University of Electronic Science and Technology of China, Chengdu 611731, China.

[e] Department of Civil and Structural Engineering, The University of Sheffield, Mappin Street, Sheffield, S1 3JD, England.

[f] Department of Mechanical and Industrial Engineering, NTNU – Norwegian University of Science and Technology, Trondheim, Norway.

*Corresponding author: ritardantas@gmail.com; jacorreia@fe.up.pt

ABSTRACT

Multiaxial stresses are usually present in engineering structures and are often associated to multiaxial fatigue failures. However, multiaxial fatigue is an open topic, full of questions and different points of view. Therefore, an experimental campaign of uniaxial and multiaxial fatigue tests under proportional loading was conducted aiming at evaluating the multiaxial fatigue behaviour of S355 structural steel in the high-cycle fatigue regime. Five different multiaxial models were used and evaluated, namely the Sines, Findley, McDiarmid, Dang Van and Susmel-MWCM. Each of them was applied to experimental data and the mean fatigue curves obtained from it were evaluated and compared. The coefficients present in each model definition were studied and determined through different methods. The Dang Van's multiscale approach and Susmel model showed great accuracy in the description of the fatigue behaviour of the S355 steel, providing the best correlation of the uniaxial and multiaxial experimental data.

KEYWORDS: Multiaxial Fatigue; High-Cycle Regime; Proportional Loading; Damage Parameters; Structural Steels.

NOMENCLATURE

$\tau_{a,oct}$ - octahedral shear stress

s- Sines' model damage parameter

k_s – Sines' constant

$\sigma_{h,mean}$ - hydrostatic mean stress

$\sigma_{1,mean}, \sigma_{2,mean}, \sigma_{3,mean}$ – principal hydrostatic mean stresses

$\sigma_{1,a}$, $\sigma_{2,a}$, $\sigma_{3,a}$ – principal stress amplitudes

$\sigma_{a,R=-1}$ - uniaxial tensile/bending fatigue stress limit amplitude for R=-1

$\sigma_{a,R=0}$ - uniaxial tensile/bending fatigue stress limit amplitude for *R=0*

$\tau_{\theta a}$ – maximum shear stress amplitude on a θ plane

$\sigma_{\theta,max}$ – maximum normal stress on a θ plane

k_f – Findley's constant

f- Findley's model damage parameter

$\tau_{a,R=-1}$ – uniaxial torsional fatigue stress limit amplitude for *R=-1*

$\sigma_{a,R=0.5}$ - uniaxial tensile/bending fatigue stress limit amplitude for *R=-0.5*

σ_u – ultimate tensile strength

$t_{A,B}$ – McDiarmid's material constant for case A or case B

$\bar{\tau}_{meso,max,d}(t)$ – maximum mesoscopic deviatoric shear stress tensor

k_d – Dang Van's constant

$\bar{\sigma}_{meso,h}(t)$ - mesoscopic hydrostatic stress tensor

d – Dang Van's damage parameter

$\bar{\sigma}_{meso,1,d}(t)$, $\bar{\sigma}_{meso,3,d}(t)$ – maximum and minimum principal mesoscopic deviatoric tensors

$\tau_{a,max}$ –maximum shear stress amplitude

$\sigma_{h,max}$ – maximum hydrostatic stress

τ_a - shear stress amplitude

N_f – number of cycles until failure

$\sigma_{n,m}$ - normal mean stress to the critical plane

τ_a^*, $\sigma_{n,m}^*$ and $\sigma_{n,a}^*$ - shear stress amplitude, the normal mean stress and the normal stress amplitude to the critical plane for an endurance limit with a stress ratio larges than -1

ρ_{eff} - effective value of the critical plane stress ratio

$\tau_{a,ref}$ - fatigue endurance limit

k_τ- negative inverse slope

$N_{f,e}$ - estimated number of cycles to failure

a, b, α and β – Susmel's material constants

$\sigma_{n,a}$- normal stress amplitude to the critical plane

ρ_{lim} – limit value imposed to ρ_{eff}

k_0 - negative inverse slope for $\rho_{eff} = 0$

k - negative inverse slope for $\rho_{eff} = 1$

$\tau_{a,0}$ - fatigue endurance limit for $\rho_{eff} = 0$

$\frac{\sigma_{a,1}}{2}$ - fatigue endurance limit for $\rho_{eff} = -1$

m – mean stress sensitivity index

E - young modulus

f_y – yield strength

f_u – tensile strength

σ_a- normal stress amplitude

R- stress ratio

R^2 - coefficient of determination

B and τ_f' – constants from Basquin's law

$\sigma_\theta, \sigma_x, \tau_{xy}$ and τ_θ - shear and normal stress components

μ - mean

σ - standard deviation

$\bar{e}$ -mean of module of error index

f - probability density function

n - number of specimens

1. INTRODUCTION

Fatigue is a critical degradation process affecting engineering structures and it is believed to be responsible for half of the failures [1]. The American Society for Testing and Materials (ASTM) defines fatigue as "*The process of progressive localized permanent structural change occurring in a material subjected to conditions that produce fluctuating stresses and strain at some point or points and that may culminate in cracks or complete fracture after a sufficient number of fluctuations*" [2]. It was first identified at the end of the nineteenth century and started to gain attention with studies conducted by Wöhler, Basquin and others. Since these pioneer observations, different approaches and models have been proposed [3].

Throughout fatigue history, it is observed a major development of uniaxial fatigue models, but a cyclic loading is even more critical when causes a complex multiaxial stress state [4]. Besides, multiaxiality is frequently observed in many engineering applications, such as wind turbines, offshore structures and bridges, due not only to complex loadings but also to notches and geometries that originate a multiaxial stress state in the presence of a uniaxial loading [1]. A multiaxial fatigue loading can be described as proportional or non-proportional. During a proportional loading, the principal stress directions do not change as consequence of in-phase loads, while a non-proportional loading originates principal stress directions which change over time, because of the out-of-phase loads. This loading characteristic results in different fatigue behaviours, and, consequently, requests specific approaches and models [1], [5].

One of the first multiaxial fatigue models was elaborated by Gough and Pollard in the 1930s and defines different failure conditions for brittle and ductile materials [6]. Along with this model, they performed a large number of biaxial fatigue tests with bending and torsional loads, which supported and inspired the formulation of others such as Findley's [7] and Sines' models [8], [9] in the 1950s. These models introduced new approaches based on the influence of different variables and concepts, such as mean stresses, stress amplitudes and critical planes, which subsequently also conduct to other models such as the one presented by Matake [10], [11]. However, these approaches were based on stresses and did not include strain values, since they were mainly focused on the region of a large number of cycles until failure [12]. The classical models developed for monotonic loadings, such as von Mises, Maximum Principal stress or Tresca were also adapted and used to assess a multiaxial fatigue stress states [5].

In 1973, Brown and Miller proposed a model that included the effect of shear and normal strains and a critical plane where shear is maximum [13], [14]. Moreover, damage models based on energy and strains appeared and became widely used, such as the Smith Watson and Topper's (SWT) [15] or the Fatemi-Socie's models [16].

The assessment of non-proportional loadings has always been a concern of fatigue research and, consequently, some models, such as McDiarmid and Lee, were formulated in order to include the effect of this kind of loads [17], [18].

Lately, new modern models have arisen such as Dang Van's multi-scale approach, which proposes a model based on the interaction between macroscopic and mesoscopic scales [19]. This model is mainly used to evaluate multiaxial fatigue stress states in rolling contact stresses and, during the last years, it has been applied to assess fatigue damage in offshore and other engineering structures [20]–[23].

Furthermore, Papadopoulos and Carpinteri-Spagnoli developed modern models with more complex approaches for hard metals. Papadopoulos' model was developed for non-proportional bending and torsion and includes details about material's crystalline structure. Since its formulation is defined by integrals, this model implies long computational times. On the other hand, the Carpinteri-Spagnoli's model defines a critical plane based on the material fatigue properties and the average of principal stress directions calculated through weight functions [1], [24]–[26].

In the last decades, numerous experimental works and publications have been proposed and developed about multiaxial fatigue in steel, such as the models developed by Susmel [27] and Liu-Mahadevan [1], [12], [28].

Summarizing, multiaxial models can be generally divided into three major groups: stress, strain and energy-based models. The last ones mentioned are also called strain-energy models and, sometimes, are included in the strain-based approaches [5]. The strain-based models are usually applied to Low-Cycle Fatigue (LCF) regime, while stress approaches are adopted to High-Cycle Fatigue (HCF) regime [5], [29], [30]. The low-cycle fatigue regime is characterized by high loads and a short fatigue life, which is usually less than 10^4cycles. In this regime, material suffers a plastic deformation since the first cycle. On the other hand, during high-cycle regime, an elastic deformation state is observed as well as longer life, usually between 10^4 and 10^7 cycles. In the last years, other fatigue regimes have been a matter of study, such as very-high cycle fatigue or ultra-low cycle fatigue [5].

Hence, this work aims at evaluating and comparing the ability of different multiaxial fatigue models to assess and portray the fatigue behaviour of S355 steel in the high-cycle fatigue regime. Firstly, some stress-based models were selected. Afterwards, an experimental campaign was defined and carried out. The experimental data is then used to assess the quality of the selected multiaxial fatigue models. Finally, the most suitable multiaxial fatigue models to evaluate the fatigue damage observed in S355 steel are selected. Since the focus of this paper is the proportional loading of constant amplitude, material mechanisms associated with more complex loadings, such as non-proportional or variable amplitude, will not be mentioned or studied.

2. OVERVIEW OF MULTIAXIAL FATIGUE MODELS

Since this work aims at evaluating the fatigue behaviour of the S355 structural steel in the high- cycle fatigue regime, experimental results were analysed and assessed through the application of stress-based models. These models can be sorted by empirical, equivalent stress and critical plane models [5]. The empirical models were the first ones to be developed and are related to experimental fatigue data. The equivalent stress models are based on static yield criteria and turn a multiaxial fatigue stress state into an equivalent uniaxial stress state [4]. Finally, the critical plane models rely on the definition of a critical plane, where the probability of crack initiation is higher [31].

Thus, five multiaxial fatigue models – Sines, Findley, McDiarmid, Dang Van, and Susmel – were considered and applied to the experimental data obtained within the scope of this work. In the following subsections, these models are presented and discussed.

2.1. Stress-Based Multiaxial Fatigue Models

2.1.1. Sines criterion

Sines [8], [9] proposed an equivalent stress model sensitive to mean stress effect. However, it cannot be applied to non-proportional loading. Hence, this model states that failure occurs when Eq. (1) is verified:

$$\tau_{a,oct} + k_s\left(3\,\sigma_{h,mean}\right) = s, \tag{1}$$

where, s is a material constant proportional to the fatigue limit, k_s is also a material constant, $\sigma_{h,mean}$ is the hydrostatic mean stress determined by Eq. (2):

$$\sigma_{h,mean} = \frac{\sigma_{1,mean}+\sigma_{2,mean}+\sigma_{3,mean}}{3}, \quad (2)$$

and $\tau_{a,oct}$ is the octahedral shear stress defined as:

$$\tau_{a,oct} = \frac{1}{3}\sqrt{(\sigma_{1,a}-\sigma_{2,a})^2+(\sigma_{2,a}-\sigma_{3,a})^2+(\sigma_{1,a}-\sigma_{3,a})^2}\ , \quad (3)$$

where, $\sigma_{1,a}$, $\sigma_{2,a}$ and $\sigma_{3,a}$ are the principal stress amplitudes.

The material constant k_s can be estimated through Eq. (4):

$$k_s = \frac{\sqrt{2}}{3}\left(\frac{\sigma_{a,R=-1}-\sigma_{a,R=0}}{\sigma_{a,R=0}}\right), \quad (4)$$

where, $\sigma_{a,R=-1}$ is the uniaxial tensile fatigue stress limit amplitude for *R=-1*, and $\sigma_{a,R=0}$ is the uniaxial tensile fatigue stress limit amplitude for *R=0*. However, this constant will be discussed in Section 5.

2.1.2. Findley criterion

Findley [7] proposed the first critical plane approach. This criterion assumes shear stress as the primary mechanism of fatigue damage and responsible for nucleation and initiation, while the normal stress is the secondary mechanism since only affects the capability of a material to withstand cyclic loading. This model considers the effect of mean stress.

The critical plane is defined as the plane where a certain damage parameter achieves the maximum value. The damage parameter is defined by the left side of Eq. (5) and the failure occurs when this equation is verified:

$$(\tau_{\theta a} + k_f\sigma_{\theta,max})_{max} = f, \quad (5)$$

where, $\tau_{\theta a}$ is the maximum shear stress amplitude on a θ plane, $\sigma_{\theta,max}$ is the maximum normal stress on a θ plane and k_f is a material constant that manages the influence of normal stress on fatigue life.

The value of k_f can be estimated by Eqs. (6) to (8) [32]:

$$\frac{\sigma_{a,R=-1}}{\tau_{a,R=-1}} = \frac{2}{1+\frac{k_f}{\sqrt{1+k_f^2}}}, \tag{6}$$

$$\frac{\sigma_{a,R=0}}{\sigma_{a,R=-1}} = \frac{k_f+\sqrt{1+k_f^2}}{2k_f+\sqrt{1+(2k_f)^2}}, \tag{7}$$

$$\frac{\sigma_{a,R=0.5}}{\sigma_{a,R=-1}} = \frac{k_f+\sqrt{1+k_f^2}}{4k_f+\sqrt{1+(4k_f)^2}}, \tag{8}$$

where, $\tau_{a,R=-1}$ is the shear stress fatigue limit amplitude for *R=-1*, and $\sigma_{a,R=0.5}$ is the normal stress fatigue limit for *R=-0.5*. As happens with Sines model constant, k_f determination and value are controversial and will be discussed in the following sections.

2.1.3. McDiarmid criterion

McDiarmid [17], [33] presented a critical plane approach that can be applied to non-proportional loading and includes the mean stress effect. According to this model, the critical plane is the one where shear stress amplitude achieves the maximum value. This model distinguishes two different cases: a case A characterized by crack growth along the surface and a case B where the crack grows inwards from the surface.

Hence, fatigue failure criterion is achieved when (Eq. (9)):

$$\frac{\tau_{\theta,a}}{t_{A,B}} + \frac{\sigma_{\theta,max}}{2\sigma_u} = 1, \tag{9}$$

where, σ_u is the ultimate tensile strength, and $t_{A,B}$ is a material constant which value is t_A or t_B for case A or case B that are the values of the reversed shear stresses for each of the different cases of crack growth.

2.1.4. *Dang Van's multi-scale approach*

Dang Van [19] developed a model based on macroscopic and mesoscopic scale concepts, assuming that before crack initiation, an elastic shakedown occurs. This material phenomenon is related to high-cycle fatigue since it is a stabilized elastic response, which only happens when yield strength is not achieved.

Besides, accordingly to this model cracks initiate in transgranular slip bands due to local shear stress and are influenced by hydrostatic pressure.

Hence, failure occurs when the following condition is verified (Eq. (10)):

$$max\left(\bar{\tau}_{meso,max,d}(t) + k_d \bar{\sigma}_{meso,h}(t)\right) = d, \tag{10}$$

where, $\bar{\sigma}_{meso,h}(t)$ is the mesoscopic hydrostatic stress tensor, k_d and d are material constants, and $\bar{\tau}_{meso,max,d}(t)$ is given by (Eq. (11)):

$$\bar{\tau}_{meso,max,d}(t) = \frac{\bar{\sigma}_{meso,1,d}(t) - \bar{\sigma}_{meso,3,d}(t)}{2}, \tag{11}$$

where, $\bar{\sigma}_{meso,1,d}(t)$ and $\bar{\sigma}_{meso,3,d}(t)$ are the maximum and minimum principal mesoscopic deviatoric tensors.

Some years later, Dang Van and Maitournam [21] proposed a simplified version of this model for engineering approaches, which is given by Eq. (12):

$$\tau_{a,max} + k_d \sigma_{h,max} = d, \tag{12}$$

where, $\tau_{a,max}$ is the maximum shear stress amplitude, and $\sigma_{h,max}$ is the maximum hydrostatic stress. The value of $\tau_{a,max}$ is not affected by mean stress, while $\sigma_{h,max}$ includes the effect of it. The material constant k_d, which will be discussed throughout this work, is usually estimated through Eq. (13) or is considered equal to the slope of a linear regression applied to axial fatigue limits for *R=0* or *R=-1* plotted in a graph $\tau_{a,max}$ versus $\sigma_{h,max}$.

$$k_d = 3\left(\frac{\tau_{a,R=-1}}{\sigma_{a,R=-1}} - \frac{1}{2}\right), \tag{13}$$

2.1.5. Modified Wöhler Curve Method

Since 2002, Susmel has been developing and proposing a critical plane approach which consists on a Modified Wöhler Curve Method (MWCM) [34], [35]. This model is based on the assumption that, under constant loading, the fatigue damage and the probability of crack initiation achieve their maximum value on the material plane that experiences the maximum shear stress amplitude, which is called "the critical plane"[34]–[40].

Therefore, the damage evaluation of this model can be summarized by a modified Wöhler diagram, which plots the shear stress amplitude on the critical plane (τ_a) versus the number of cycles until failure (N_f)(Fig.1). The design curves of this diagram are characterised by two variables: the negative inverse slope ($k_\tau(\rho_{eff})$), and the fatigue endurance limit ($\tau_{a,ref}(\rho_{eff})$) at a certain defined number of cycles to failure (N_{ref}). Both variables mentioned above are characterised by a third variable: the effective value of the critical plane stress ratio (ρ_{eff}), which is given by Eq. (14):

$$\rho_{eff} = \frac{m \cdot \sigma_{n,m} + \sigma_{n,a}}{\tau_a}, \tag{14}$$

where τ_a is the shear stress amplitude, $\sigma_{n,m}$ is the normal mean stress, $\sigma_{n,a}$ is the normal stress amplitude, to the critical plane, and m is the mean stress sensitivity index and a material property, which varies between 0 and 1 [39]. The index m can be determined through Eq. (15):

$$m = \frac{\tau_a^*}{\sigma_{n,m}^*}\left(2\frac{\tau_{a,R=-1} - \tau_a^*}{2\tau_{a,R=-1} - \sigma_{a,R=-1}} - \frac{\sigma_{n,a}^*}{\tau_a^*}\right), \tag{15}$$

where τ_a^*, $\sigma_{n,m}^*$ and $\sigma_{n,a}^*$ are the shear stress amplitude, the normal mean stress and the normal stress amplitude to the critical plane for an endurance limit with a stress ratio larges than -1, while $\tau_{a,R=-1}$ and $\sigma_{a,R=-1}$ are the fully reversed fatigue limits for a uniaxial and a torsional loading case [40]. Thus, in order to determine this material property, three different endurance limits are required and when they are not known, it is assumed that the material under study is fully sensitive to normal mean stress and m is assumed to be equal to 1 [40].

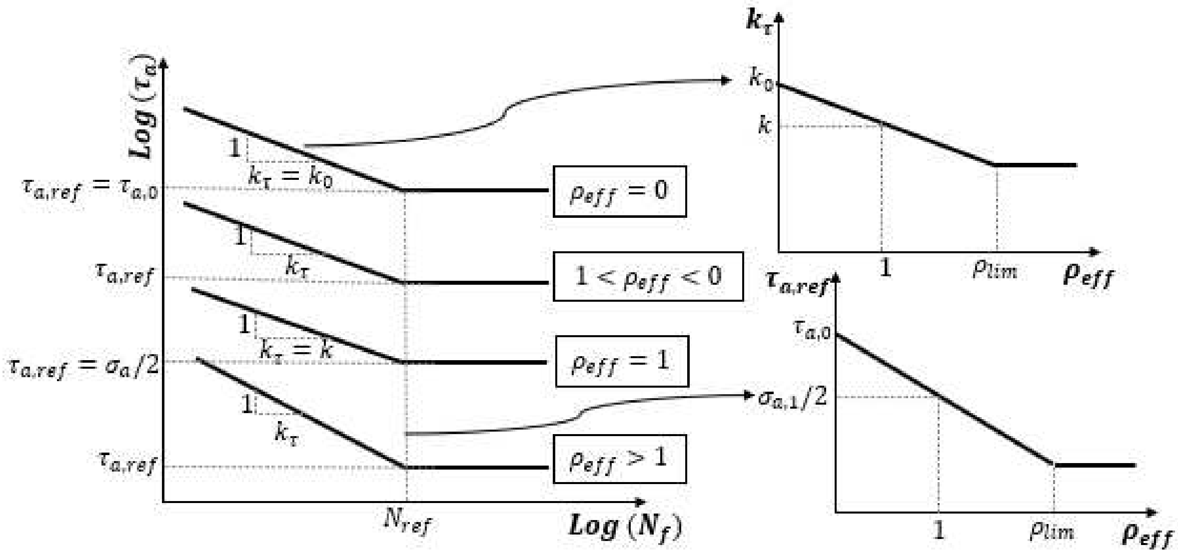

Figure 1. Modified Wöhler diagram, $k_\tau vs\ \rho_{eff}$ and $\tau_{A,Ref} vs\ \rho_{eff}$ curves [36]

As can be seen in Fig. 1, there is a singular design curve for each loading scenario associated with the corresponding ρ_{eff} value which, as mention above, originates also different pairs of $\tau_{a,ref}(\rho_{eff})$ and $k_\tau(\rho_{eff})$ values, that define each curve. These curves are defined by Eq. (16), which gives the estimated number of cycles to failure ($N_{f,e}$):

$$N_{f,e} = N_{ref} \cdot \left[\frac{\tau_{a,ref}(\rho_{eff})}{\tau_a}\right]^{k_\tau(\rho_{eff})}, \tag{16}$$

As can be seen in equation above as well as in Eq. (14), the ratio ρ_{eff} has a significant role in fatigue life estimation and portrays the non-zero mean stresses, the degree of multiaxiality and the non-proportionality of the loading history. Furthermore, it is important to mention that $\rho_{eff}$is always equal to unity under fully-reversed uniaxial fatigue loading and equal to zero under fully-reversed torsional fatigue loading, which is helpful to calibrate the model [36].

Finally, the $k_\tau(\rho_{eff})$ and $\tau_{a,ref}(\rho_{eff})$ can be determined through Eqs. (17) and (18):

$$k_\tau(\rho_{eff}) = \alpha \cdot \rho_{eff} + \beta, \tag{17}$$

$$\tau_{a,ref}(\rho_{eff}) = a \cdot \rho_{eff} + b, \tag{18}$$

where a, b, α and β are material fatigue constants. By calibrating the above equations through the fully reversed uniaxial $\left(\rho_{eff} = 1; k_\tau(\rho_{eff} = 1) = k; \tau_{a,ref}(\rho_{eff} = 1) = \frac{\sigma_{a.1}}{2}\right)$ and torsional ($\rho_{eff} = 0; k_\tau(\rho_{eff} = 0) = k_0; \tau_{a,ref}(\rho_{eff} = 0) = \tau_{a,0}$) fatigue curves, Eqs. (17) and (18) can be rewritten as:

$$k_\tau(\rho_{eff}) = (k - k_0)\rho_{eff} + k_{0,} \text{ for } \rho_{eff} \leq \rho_{lim} \tag{19}$$

$$k_\tau(\rho_{eff}) = (k - k_0)\rho_{lim} + k_0, \text{ for } \rho_{eff} > \rho_{lim} \tag{20}$$

$$\tau_{a,ref}(\rho_{eff}) = \left(\frac{\sigma_{a,1}}{2} - \tau_{a,0}\right)\rho_{eff} + \tau_{a,0} = const. \text{ for } \rho_{eff} \leq \rho_{lim} \tag{21}$$

$$\tau_{a,ref}(\rho_{eff}) = \left(\frac{\sigma_{a,1}}{2} - \tau_{a,0}\right)\rho_{lim} + \tau_{a,0} = const. \text{ for } \rho_{eff} > \rho_{lim} \tag{22}$$

where ρ_{lim} is a limit value imposed to ρ_{eff}, since this model becomes too conservative for high values of ρ_{eff}.and can be calculated through Eq. (23) [35]:

$$\rho_{lim} = \frac{\tau_a}{2\tau_{a,0} - \sigma_a} \tag{23}$$

3. Experimental Programme

An experimental campaign was defined and carried out with the objective of obtaining mean fatigue curves and analysing each multiaxial fatigue model. Therefore, uniaxial and biaxial fatigue tests were performed using smooth hourglass specimens made of S355 structural steel, with a minimum cross section of 44.18 mm^2 (Fig. 2 (a)). The mechanical properties and chemical composition of the tested S355 steel are listed in Tables 1 and 2, respectively. The hardness was measured and determined through a sample which was cut from a specimen, while the other mechanical properties were collected from [41], [42]. The microstructure was also analysed, and a ferrite-pearlite microstructure is observed, as portrayed in Figure 2 (b).

Table 1. Mechanical Properties of S355 steel [42][41]

Young Modulus (E) *GPa*	*Yield Strength (f_y)* *MPa*	*Tensile Strength (f_u)* *MPa*	*Hardness* *HV10*
211.60	367	579	151.28

Table 2. Chemical composition of S355 steel [42]

C *%*	*Cu* *%*	*Mn* *%*	*N* *%*	*P* *%*	*S* *%*	*Si* *%*
0.16	0.2	1.28	0.009	0.03	0.02	0.3

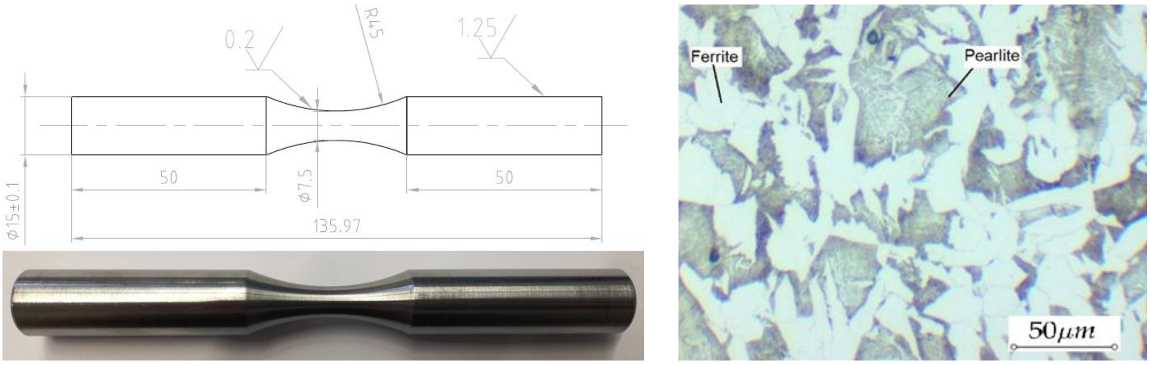

(**a**) (**b**)

Figure 2. (a) Hourglass specimen (in mm) [42]; (b) Microstructure of S355 steel (Magn. 400×) [42].

Hence, nineteen uniaxial and eighteen biaxial fatigue tests were conducted for different stress ratios: *R=0.01* and *R=-1*. During axial tests, a cyclic axial force was applied to the specimen, while in the biaxial tests both cyclic torsional torque and a cyclic axial force were applied in-phase. In sixteen biaxial tests, the shear stress caused by the torque was half of the normal stress originated by the force, while in the rest of the tests they were equal, in order to evaluate the effect of shear stress in fatigue life. The loads were applied according a frequency of *10 Hz* following sinusoidal functions of constant amplitude over time.

Both types of test were carried out in force control, using a MTS 810 testing system, which can apply a maximum axial force of *100kN*, for axial tests, and a MTS 809 Axial/torsional test system, which is characterized by a maximum axial capacity of 50 kN and a maximum torsional capacity of *0.5 kN.m*, for biaxial tests (refer to Figs. 3 (a) and (b)).

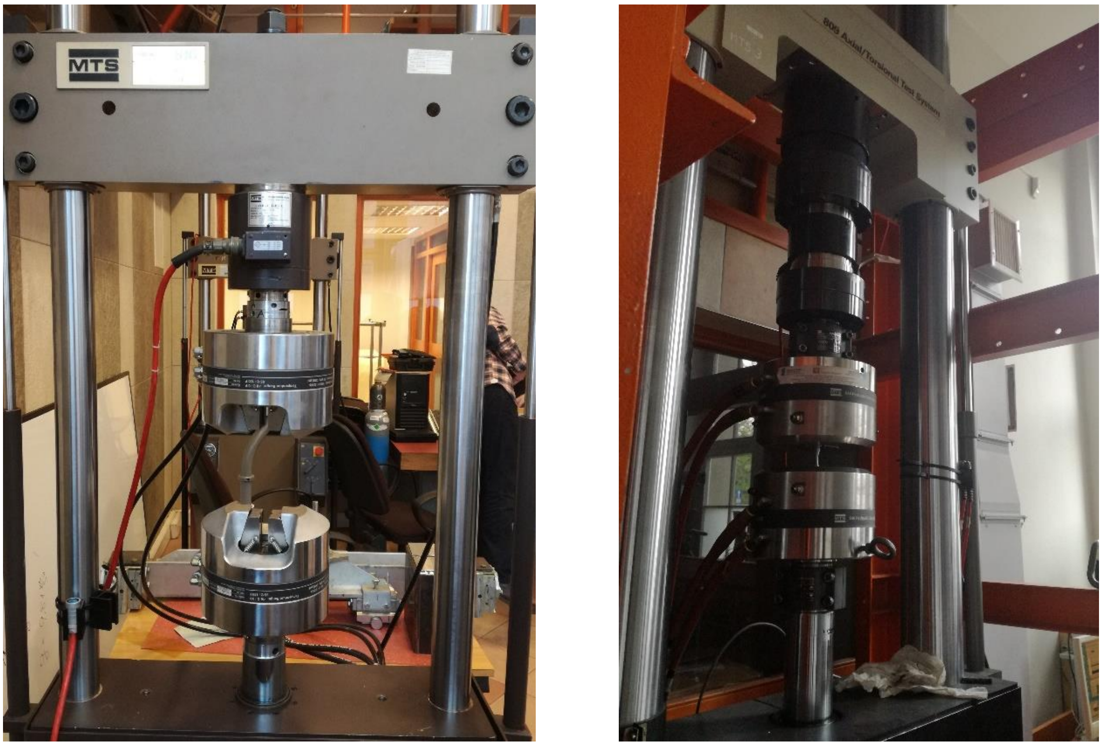

(a) (b)

Figure 3. Testing system machines: (a) MTS 810 testing system [42]; (b) MTS 809 Axial/torsional test system [42].

For each test, the number of cycles until failure and the level of loading applied were recorded. For each loading level, only two experimental tests were carried out due to the limited material available. It was assumed run-out and the test interrupted when 5000000 cycles were achieved without the specimen failure [42].

4. EXPERIMENTAL RESULTS

The results obtained for each fatigue test are listed in Table 3, which includes the loading mode, the stress R-ratio, normal and shear stress amplitudes and the number of cycles until specimen failure. These results show the effect of stress ratio or in other words the effect of a mean stress, in fatigue life as well as how much a biaxial stress state can be more severe than a simple uniaxial one. Furthermore, in the last biaxial tests, where the shear stress was increased, it is visible the impact of this kind of stress on fatigue life.

Besides, the specimens' fracture surfaces were observed and analysed with an optical microscope aiming at identifying some differences between loading conditions. Thus, Figs. 4 to 8 depict the fracture behaviour and respective surfaces for each kind of loading. The crack initiation origin is marked with an 'O' when is easily identified and is constrained to a single region, which is the case of specimens tested under axial loading (Figs. 4 and 5) and proportional loading with stress ratio close to 0 (Fig. 5). On the other hand, as can be seen in Figs. 7 and 8, specimens under fully reversed proportional loading, there are multiple crack initiation origins, probably due to the shear stress effect.

In Fig. 4 (a), the fatigue and overload zones are easily distinguished, since it is noticeable the increase of roughness between them. Furthermore, a ratchet is marked with the letter 'R', while in Fig. 5 (a) river marks are observed, which dictates the direction of crack propagation and are identified with a letter 'M'.

Another relevant aspect is the difference observed between the fracture surface of Figs. 7 (a) and 8(b), which highlights the impact of the shear stress caused by the torsional loading. Moreover, the influence of stress R-ratio is observed in the fractures: only the specimens which were tested under R=0.01 show an elongation and in the others, the fracture remains closed after test (Figs. 4(b), 5(b), 6(b), 7(b) and 8 (b)).

(a) (b)

Figure 4. Specimen tested under $\sigma_a = 207$ MPa (with $R = 0.01$): (a) fracture surface; (b) fracture [42].

Table 3. Results of uniaxial and biaxial fatigue tests [42].

Loading Condition	*Stress R-Ratio*	*Normal stress amplitude,* σ_a $[MPa]$	*Shear stress amplitude,* $\tau_a [MPa]$	σ_a/τ_a [-]	*Number of cycles to Failure,* N_f
Axial	0.01	168	-	∞	5000000 (∞)
Axial	0.01	182	-	∞	5000000 (∞)
Axial	0.01	188	-	∞	5000000 (∞)
Axial	0.01	190	-	∞	5000000 (∞)
Axial	0.01	193	-	∞	5000000 (∞)
Axial	0.01	196	-	∞	324373
Axial	0.01	196	-	∞	281589
Axial	0.01	202	-	∞	621182
Axial	0.01	202	-	∞	131064
Axial	0.01	207	-	∞	247161
Axial	0.01	207	-	∞	315639
Axial	0.01	216	-	∞	122047
Axial	0.01	216	-	∞	76082
Axial	-1	232	-	∞	5000000 (∞)
Axial	-1	232	-	∞	2147377
Axial	-1	249	-	∞	561786
Axial	-1	249	-	∞	406826
Axial	-1	272	-	∞	157983
Axial	-1	272	-	∞	98626
Axial+Torsional	0.01	151	75	2	5000000 (∞)
Axial+Torsional	0.01	160	79	2	5000000 (∞)
Axial+Torsional	0.01	165	82	2	5000000 (∞)
Axial+Torsional	0.01	168	84	2	332151
Axial+Torsional	0.01	168	84	2	256955
Axial+Torsional	0.01	174	87	2	313815
Axial+Torsional	0.01	174	87	2	656534
Axial+Torsional	0.01	174	87	2	181536
Axial+Torsional	-1	164	82	2	5000000 (∞)
Axial+Torsional	-1	181	90	2	5000000 (∞)
Axial+Torsional	-1	194	99	2	2546156
Axial+Torsional	-1	194	99	2	2040566
Axial+Torsional	-1	204	104	2	133962
Axial+Torsional	-1	204	104	2	835602
Axial+Torsional	-1	204	104	2	390101
Axial+Torsional	-1	204	104	2	383422
Axial+Torsional	-1	164	164	1	88165
Axial+Torsional	-1	164	164	1	44152

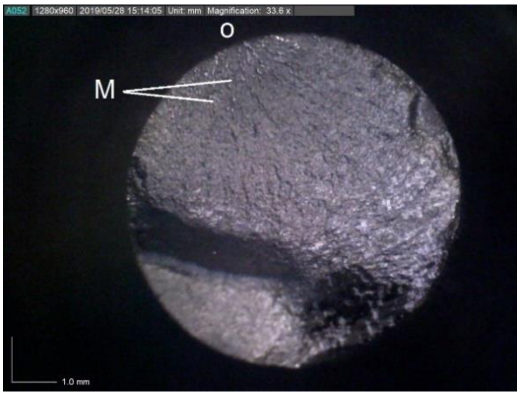

(a)

(b)

Figure 5. Specimen tested under $\sigma_a = 272$ MPa (with $R = -1$): (a) fracture surface; (b) fracture [42].

(a)

(b)

Figure 6. Specimen tested under $\sigma_a = 168$ MPa and $\tau_a = 84$ MPa (with $R = 0.01$): (a) fracture surface; (b) fracture [42].

(a)

(b)

Figure 7. Specimen tested under $\sigma_a = 204$MPa and $\tau_a = 104$ MPa (with $R = -1$): (a) fracture surface; (b) fracture [42].

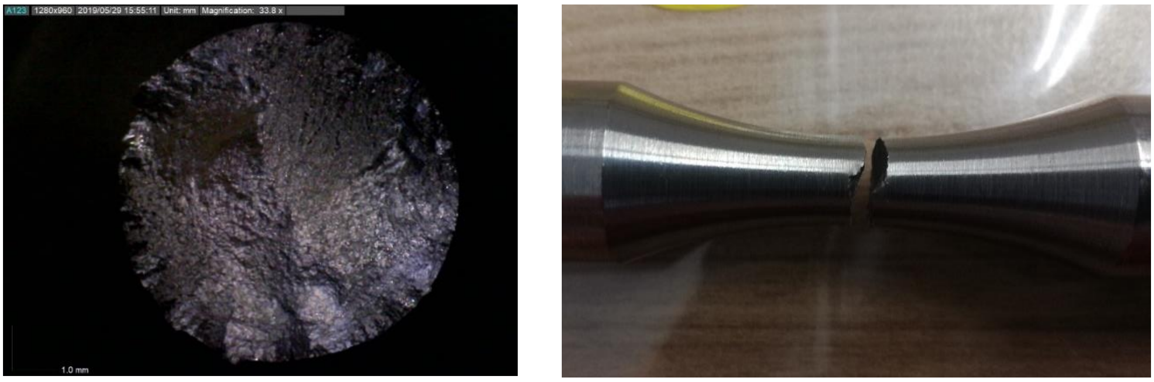

(a) (b)

Figure 8. Specimen tested under $\sigma_a = 164\text{MPa}$ and $\tau_a = 164\text{MPa}$ (with $R = -1$): (a) fracture surface; (b) fracture [42].

5. APPLICATION AND DISCUSSION

5.1. Uniaxial fatigue data

The uniaxial fatigue data obtained through the experimental campaign was plotted in a logarithmic scale and a power regression was applied according to Basquin law, in order to obtain the S-N curves. The mean fatigue curves obtained can be seen in Fig. 9 and these curves are defined by Eqs. (24) and (25), for *R=0.01* (Eq. 18) and *R=-1* (Eq. 19), respectively:

$$\begin{cases} \sigma_a = 274.49\, N_f^{-0.024} \\ R^2 = 0.507 \end{cases}, \tag{24}$$

$$\begin{cases} \sigma_a = 456.46\, N_f^{-0.045} \\ R^2 = 0.929 \end{cases}, \tag{25}$$

where R^2 is the coefficient of determination.

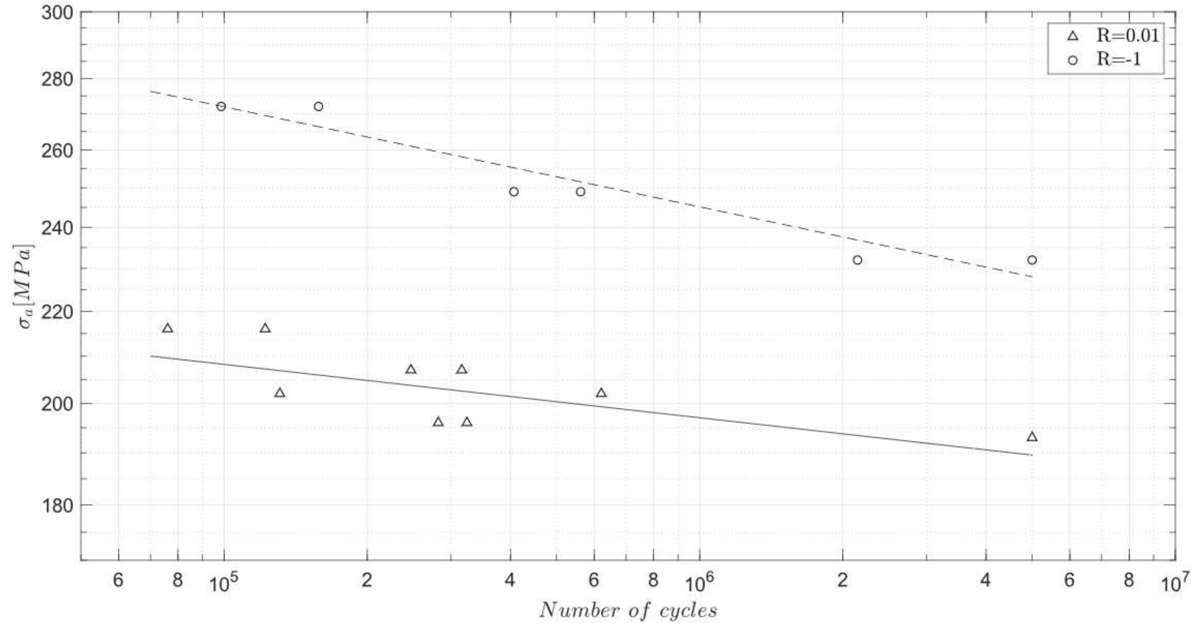

Figure 9. Mean S-N curves for axial loading under R=0.01 and R=-1 [42]

5.2. Biaxial fatigue data

The biaxial fatigue data is characterized by normal and shear stresses and, as a consequence, cannot be represented through a simple Basquin law. Thus, the multiaxial fatigue damage parameters described in the preview section aim to summarize the contribute of normal and shear stress in a single variable and then plot it as function of the number of cycles, in order to obtain suitable fatigue curves for S355 steel. Usually, a suitable multiaxial fatigue damage criterion collapses all experimental data around a design curve with a small scatter.

Hence, several multiaxial fatigue models, Sines, Findley, McDiarmid, Dang-Van and Susmel-MWCM, are considered and applied. For each model, multiaxial parameters were estimated, power regressions were performed as well as their coefficients of determination (R^2) were calculated, except for the Susmel Model which follows a different methodology from the other fatigue models.

After the determination of multiaxial fatigue design curves for each model, they were compared and evaluated, in order to select the models more and less suitable to describe fatigue life of S355 steel in the region under study.

5.2.1. Sines

In order to estimate the fatigue life of a certain loading condition, Sines model was combined with Basquin law into the following equation (Eq. (26)):

$$\tau_{a,oct} + k_s\left(3\,\sigma_{h,mean}\right) = \tau_f'(2N_f)^{B}, \qquad (26)$$

where, B and τ_f' are constants obtained through the regression analysis.

The material constant k_s can be estimated through Eq. (4), which was developed by algebraic manipulation and has the great advantage of requiring only two fatigue limits, which can be easily determined or found in the literature. However, these fatigue limits are considerable unstable. Therefore, this model was applied by assuming two different values of k_s.

Firstly, the k_s was calculated through Eq. (4), proposed by Sines [8], [9], and axial stress fatigue limits obtained in this experimental campaign ($\sigma_{a,R=-1}$= *232MPa* and $\sigma_{a,R=0}$= *193MPa*), which results in a k_s equal to *0.095*. Thus, for this value is obtained Eq. (27) and Fig. 10:

$$\begin{cases} s = 195.38\,N_f^{-0.036} \\ R^2 = 0.349 \end{cases}, \qquad (27)$$

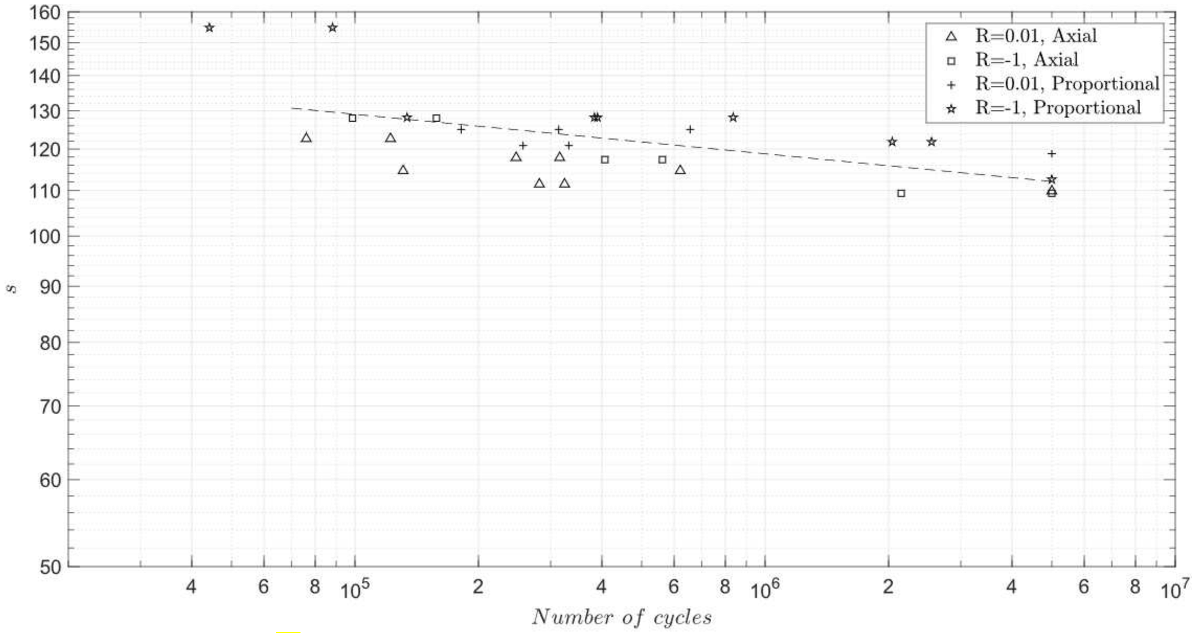

Figure 10. Sines damage parameter as function of fatigue life for $k_s = 0.095$ [42]

The second value of k_s is a result of a methodology proposed by the authors of this work and which includes all fatigue limits from the fatigue tests under uniaxial and multiaxial loading conditions for all stress ratios (R) under consideration. In this sense, a linear regression analysis to obtain the k_s parameter, with the purpose of achieving a better fit, is suggested and given by:

$$\tau_{a,oct,i} = (-3k_s) \cdot \sigma_{h,mean,i} + \tau_{a,oct,0}, \tag{28}$$

where, $\tau_{a,oct,i}$ is related to a random sample and considered a dependent variable, $\sigma_{h,mean,i}$ is the independent variable of $\tau_{a,oct,i}$, and $\tau_{a,oct,0}$ is the interception with vertical axis (the value of $\tau_{a,oct}$ when $\sigma_{h,mean} = 0$). In this analysis, a two-parameter log-normal distribution describes the $\tau_{a,oct,i}$, and the maximum likelihood estimators of $\tau_{a,oct,0}$ and $(3k_s)$ are, respectively, given by:

$$\tau_{a,oct,0} = \bar{\tau}_{a,oct} + (3k_s) \cdot \bar{\sigma}_{h,mean}, \tag{29}$$

$$(-3k_s) = \frac{\sum_{i=1}^{n}\left(\sigma_{h,mean,i} - \bar{\sigma}_{h,mean}\right)\left(\tau_{a,oct,i} - \bar{\tau}_{a,oct}\right)}{\sum_{i=1}^{n}\left(\sigma_{h,mean,i} - \bar{\sigma}_{h,mean}\right)^2}, \tag{30}$$

where, $\bar{\sigma}_{h,mean}$ and $\bar{\tau}_{a,oct}$ are the average values of the experimental fatigue limits of $\sigma_{h,mean,i}$ and $\tau_{a,oct,i}$ for several stress ratios (R) of uni- and multi-axial loading conditions, respectively, and n is the number of samples corresponding to the several stress ratios (R) and loading conditions studied and considered.

This methodology was applied based on the fatigue limits obtained in this experimental work and in ref. [43] for pure torsion, pure bending, and torsion combined with bending. All experimental fatigue limits are presented in Table 4. The function obtained based on the proposed approach is portrayed in Fig. 11 and its slope equals 0.365 corresponds to $3k_s$, which means that, accordingly to this method, $k_s = 0.122$.

Table 4. Experimental fatigue limits in $\sigma_{h,mean}$ and τ_{aoct} [42] [43]

Loading	*R*	$\sigma_{h,mean}$ *MPa*	τ_{aoct} *MPa*
Axial	0.01	66	91
Axial	-1	0	109
Axial+Torsional	0.01	56	103
Axial+Torsional	-1	0	113
Torsional	-1	0	144
Torsional	-0.5	0	105
Torsional	0	0	102
Bending	0	68	96
Bending	-0.5	23	96
Bending	-1	0	119
Bending+Torsional	0	35	99
Bending+Torsional	-0.5	12	106
Bending+Torsional	-1	0	139

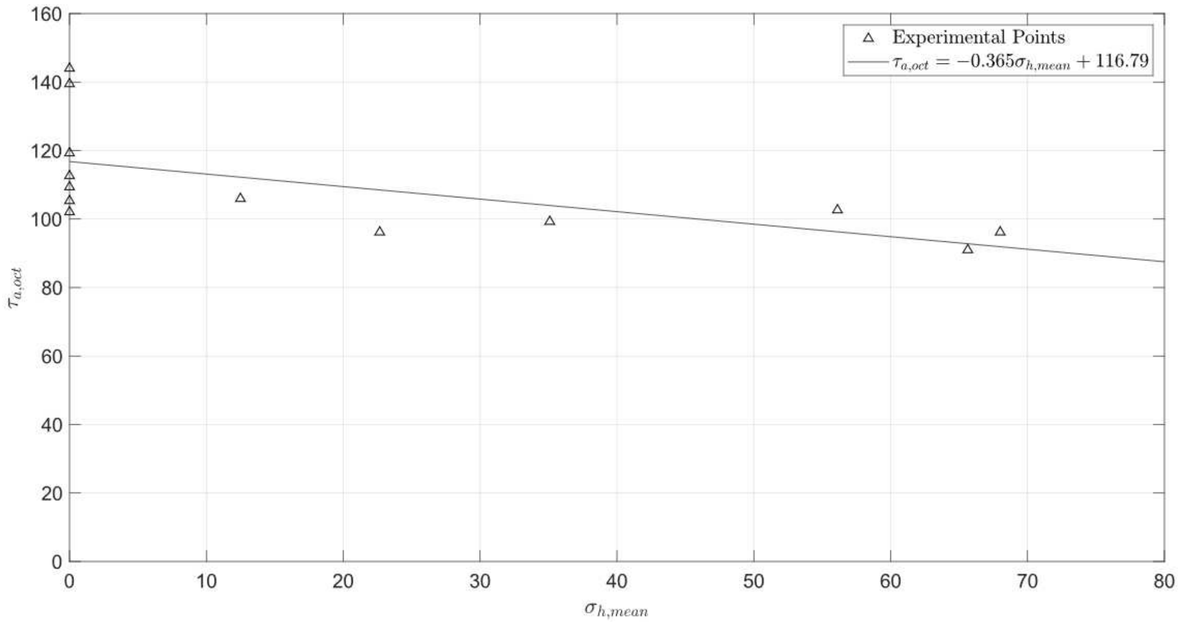

Figure 11. Graph of octahedral shear amplitude as function of hydrostatic mean stress [42]

The power regression equation and graph obtained with this k_s are the following ones (Eq. (31):

$$\begin{cases} s = 205.67\ N_f^{-0.039} \\ R^2 = 0.451 \end{cases}, \tag{31}$$

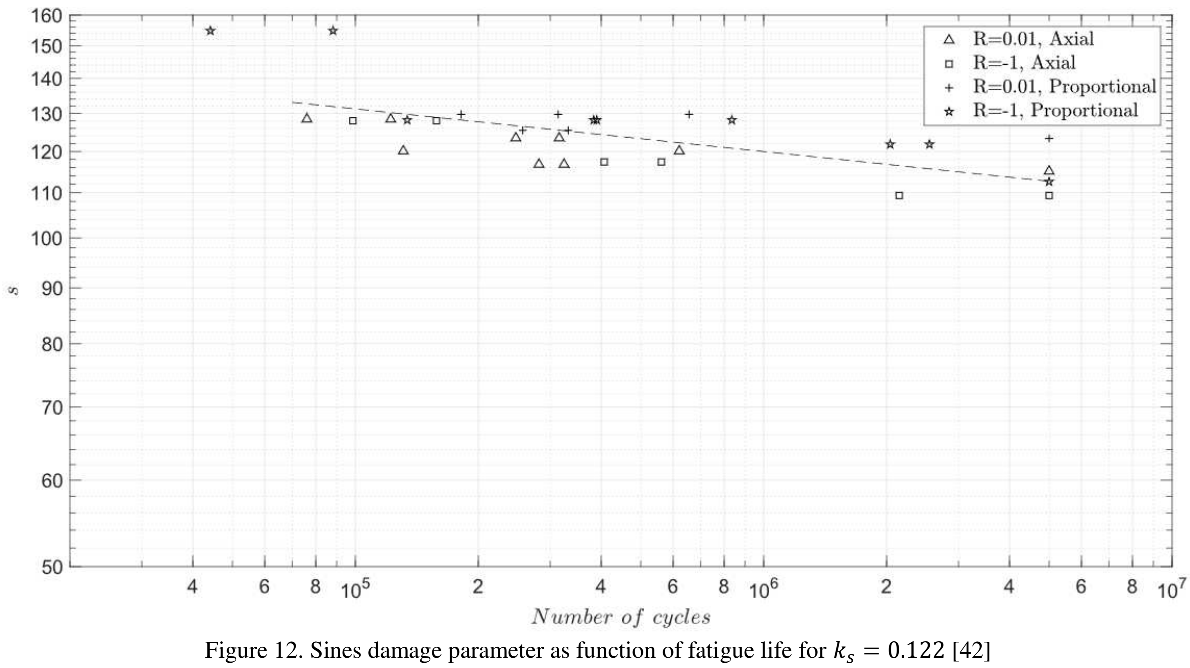

Figure 12. Sines damage parameter as function of fatigue life for $k_s = 0.122$ [42]

Summarizing, Fig. 12 shows a lower scatter of experimental points than Fig. 10, so this last method provided a better value for k_s, and, consequently, a better estimation of a fatigue curve for the S355 steel.

5.2.2. Findley

Findley's model was combined with Basquin law according to Eq. (32):

$$(\tau_{\theta a} + k_f \sigma_{\theta,max})_{max} = \tau'_f (2N_f)^B, \quad (32)$$

The critical plane of this model changes with the value of k_f and shear stress ($\tau_{\theta a}$) and normal stress ($\sigma_{\theta,max}$) must be determined in this plane, which makes the application of it more complex and difficult. Hence, these stress components were calculated for each plane (with an increment of 0.5 degrees), the respective damage parameter determined with them and, then, the maximum value and the plane where it occurs selected. The shear and normal stress were calculated using Eqs. (33) and (34) from Mohr's circle principle:

$$\sigma_\theta = \frac{\sigma_x + \sigma_y}{2} + \frac{\sigma_x - \sigma_y}{2} cos(2\theta) + \tau_{xy} sen(2\theta) \quad (33)$$

$$\tau_\theta = \frac{\sigma_x - \sigma_y}{2} cos(2\theta) - \tau_{xy} cos(2\theta) \quad (34)$$

where θ is the angle between σ_θ and σ_x, and σ_θ, σ_x, τ_{xy} and τ_θ, the shear and normal stress components defined in Fig. 13.

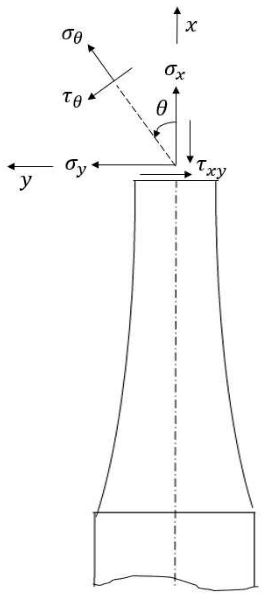

Figure 13: Definition of stress components presents on a specimen during fatigue tests [42]

Furthermore, in Eq. (32), there is an unknown constant, k_f, which was firstly determined through Eqs. (6), (7) and (8) defined in Section 2 and fatigue limits obtained in this work and in [43]. The values of k_f obtained are summarized in Table 5.

Table 5. Values of k_f considering different fatigue limits and equations [42][43]

Equations	*Fatigue limits (MPa)*	$\boldsymbol{k_f}$
$\frac{\sigma_{a,R=-1}}{\tau_{a,R=-1}} = \frac{2}{1+\frac{k_f}{\sqrt{1+k_f^2}}}$	$\sigma_{a,R=-1} = 253$ (bending) $\tau_{a,R=-1} = 176$ (torsional)	*0.425*
$\frac{\sigma_{a,R=0}}{\sigma_{a,R=-1}} = \frac{k_f+\sqrt{1+k_f^2}}{2k_f+\sqrt{1+(2k_f)^2}}$	$\sigma_{a,R=-1} = 253$ (bending) $\sigma_{a,R=0} = 204$ (bending)	*0.228*
$\frac{\sigma_{a,R=0}}{\sigma_{a,R=-1}} = \frac{k_f+\sqrt{1+k_f^2}}{2k_f+\sqrt{1+(2k_f)^2}}$	$\sigma_{a,R=-1} = 232$ (axial) $\sigma_{a,R=0} = 193$ (axial)	*0.192*

Then, mean fatigue curves equations and graphics were obtained for each value of k_f:

- $k_f = 0.425$ (Fig. 14)

$$\begin{cases} f = 365.42\ N_f^{-0.042} \\ R^2 = 0.359 \end{cases}, \tag{35}$$

- $k_f = 0.228$ (Fig. 15)

$$\begin{cases} f = 267.79\ N_f^{-0.037} \\ R^2 = 0.378 \end{cases}, \tag{36}$$

- $k_f = 0.192$ (Fig. 16)

$$\begin{cases} f = 251.65 N_f^{-0.036} \\ R^2 = 0.296 \end{cases}, \tag{37}$$

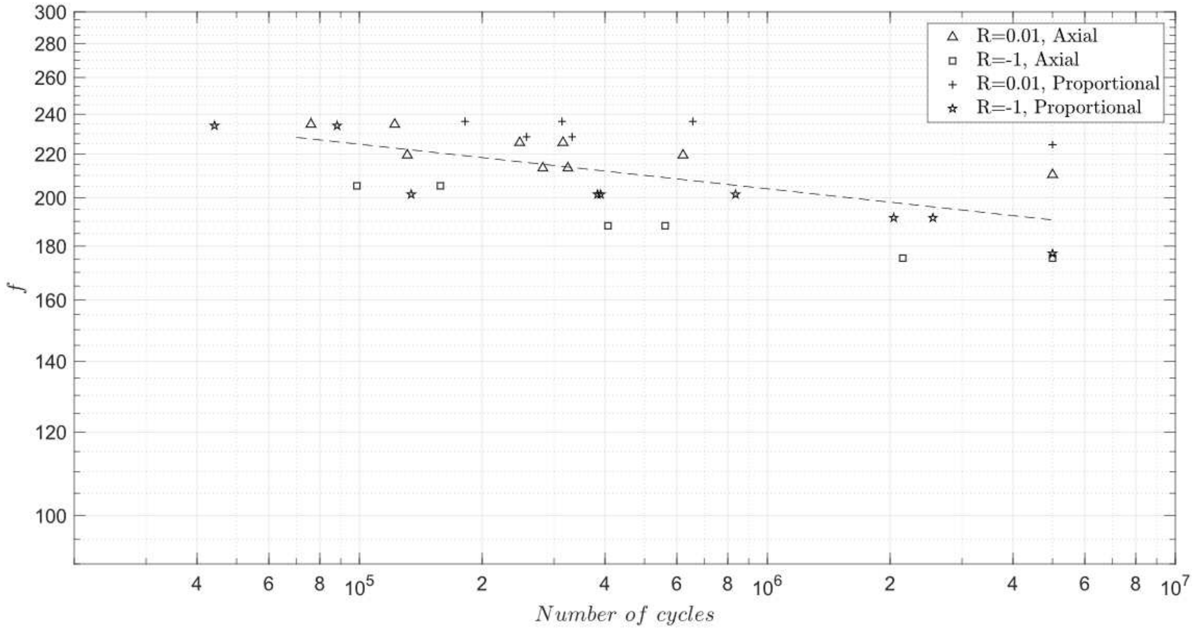

Figure 2. Findley damage parameter as function of fatigue life for $k_f = 0.425$ [42]

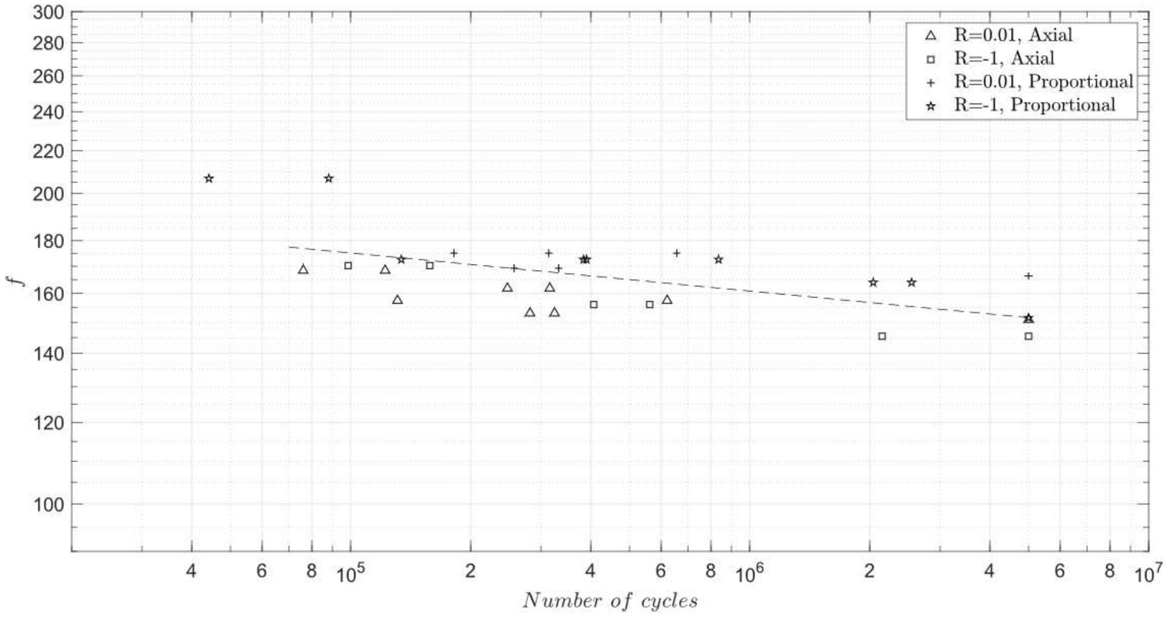

Figure 15. Findley damage parameter as function of fatigue life for $k_f = 0.228$ [42]

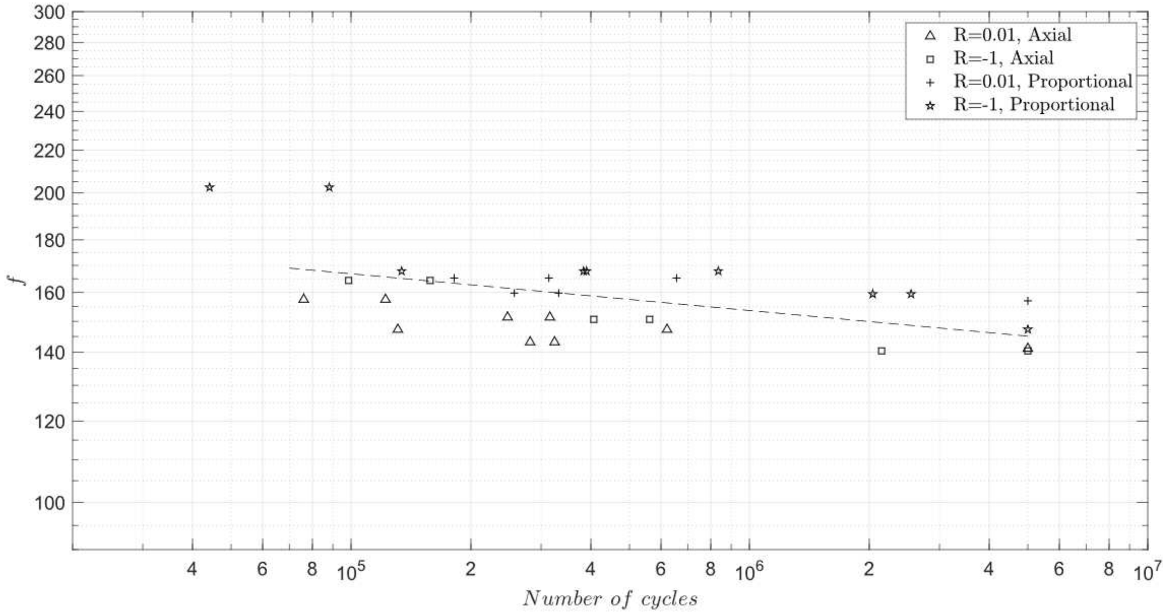

Figure 16. Findley damage parameter as function of fatigue life for $k_f = 0.192$ [42]

Thus, in Figs. 14 to 16 can be seen how the value of k_f influences the performance of the Findley's model, since the scatter changes considerably between the different values of k_f. Furthermore, the constant values obtained for each fatigue limit and equation are completely different as well as the mean fatigue curves.

Therefore, with the aim of clarifying this matter and finding a k_f value, which could achieve a lower scatter of experimental data, a new approach was developed and applied. This new methodology, aiming to estimate the enhanced Findley parameter, tries to include the mutual dependency observed between k_f and critical plane, and to find an enhanced value of k_f based on the previous ones calculated.

Since the critical plane is constant for the same kind of loading and value of k_f, for each constant value and type of loading, a point, which coordinates are listed in Table 6, was plotted in Fig. 17. Subsequently, a parallelogram was defined with the experimental points. The middle point, where the diagonals of this polygon intersect each other, define the enhanced value of k_f, which in the case of S355 steel is 0.304 [42].

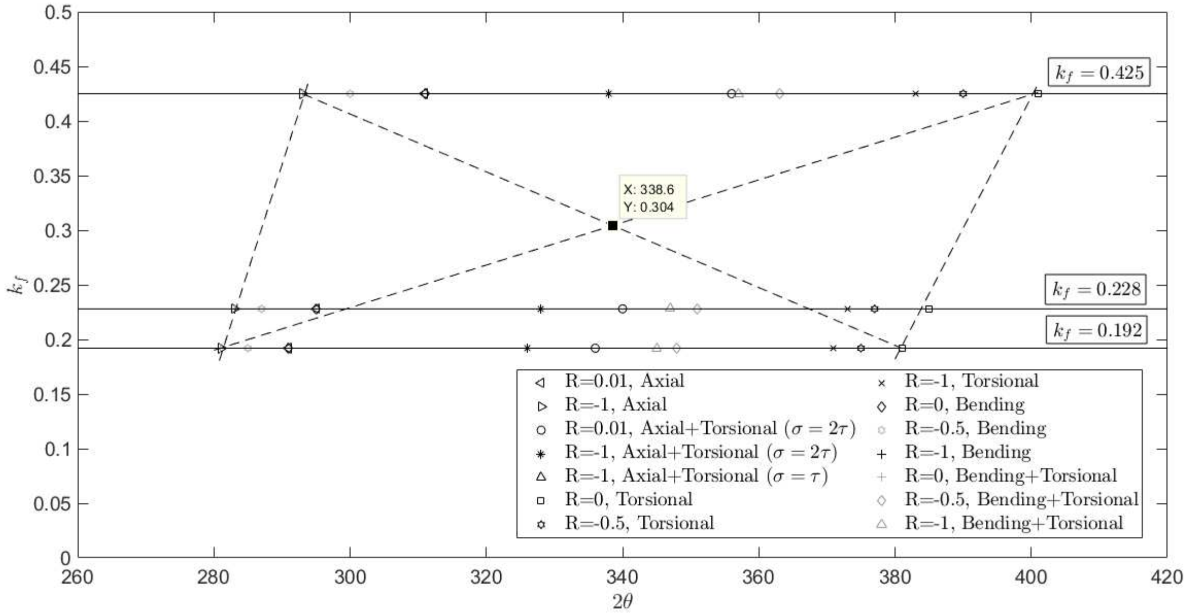

Figure 17. Scheme of the new proposed approach [42]

Table 6. Critical plane for each loading, stress ratio and k_f [42][43]

Loading	*R*	2θ ^{o}	k_f
Axial	0.01	291	0.192
		295	0.228
		311	0.425
Axial	-1	281	0.192
		283	0.228
		293	0.425
Axial+Torsional (σ=2τ)	0.1	336	0.192
		340	0.228
		356	0.425
Axial+Torsional (σ=2τ)	-1	326	0.192
		328	0.228
		338	0.425
Axial+Torsional (σ=τ)	-1	345	0.192
		347	0.228
		357	0.425
Torsional	0	381	0.192
		385	0.228
		401	0.425
Torsional	-0.5	375	0.192
		377	0.228
		390	0.425
Torsional	-1	371	0.192

		373	0.228
		383	0.425
Bending	0	291	0.192
		295	0.228
		311	0.425
Bending	-0.5	285	0.192
		287	0.228
		300	0.425
Bending	-1	281	0.192
		283	0.228
		293	0.425
Bending+Torsional	0	355	0.192
		358	0.228
		374	0.425
Bending+Torsional	-0.5	348	0.192
		351	0.228
		353	0.425
Bending+Torsional	-1	345	0.192
		347	0.228
		357	0.425

Finally, the fatigue curve for this value of k_f was obtained and plotted in Fig. 18:

$$\begin{cases} f = 303.78\, N_f^{-0.039} \\ R^2 = 0.466 \end{cases}, \quad (38)$$

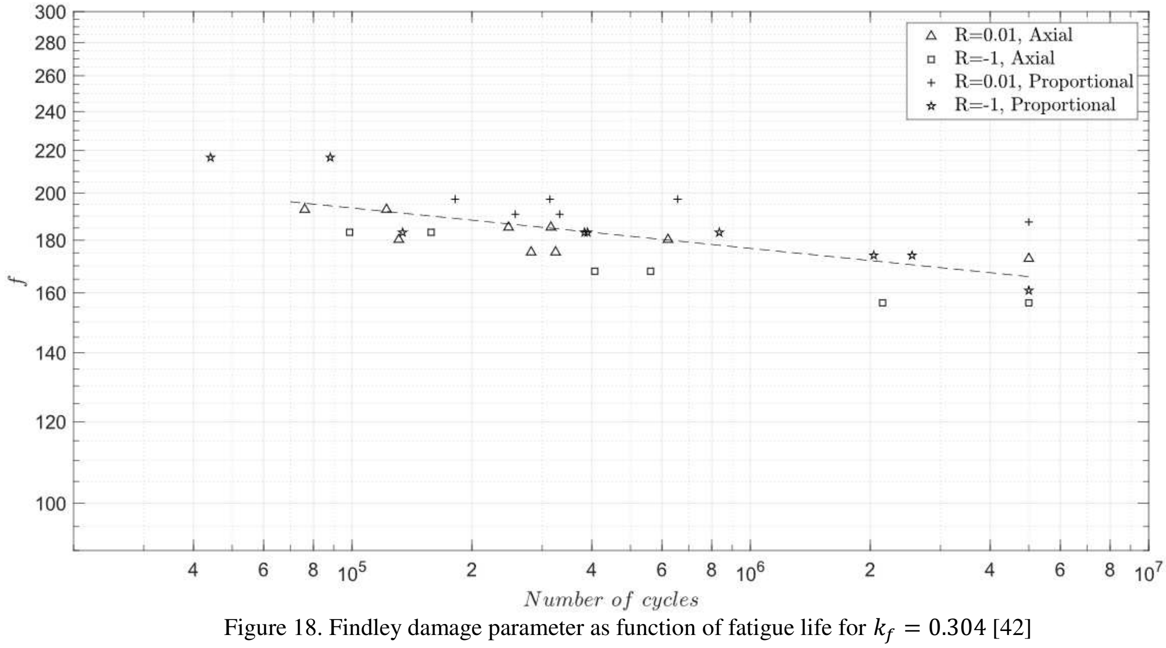

Figure 18. Findley damage parameter as function of fatigue life for $k_f = 0.304$ [42]

Although the complexity of this methodology, it resulted in the lowest scatter among the experimental fatigue data and seems to provide a suitable fatigue curve to describe S355 steel fatigue behaviour.

5.2.3. McDiarmid

The McDiarmid's model has the advantage of defining a critical plane as the one where shear stress amplitude achieves the greatest value, which is less complex in terms of application than the previous model. Furthermore, as can be seen in Eq. (39) formulated from the combination with Basquin law, there is no unknown constant:

$$\tau_{\theta,a} + \frac{\sigma_{\theta,max}}{2\sigma_u} t_{A,B} = \tau'_f (2N_f)^B, \tag{39}$$

where, $t_{A,B}$ is the fully reversed torsional fatigue limit (176 MPa), so, as consequence, $\frac{t_{A,B}}{2\,\sigma_u}$ is 0.152.

At this point, the fatigue curve equation and graph can be defined for this model (Eq. (40)):

$$\begin{cases} m = 225.61\ N_f^{-0.033} \\ R^2 = 0.173 \end{cases}, \tag{40}$$

However, as it is depicted in Fig. 19, McDiarmid provides a small correlation of the experimental fatigue data and should not be used to describe S355 steel fatigue behaviour.

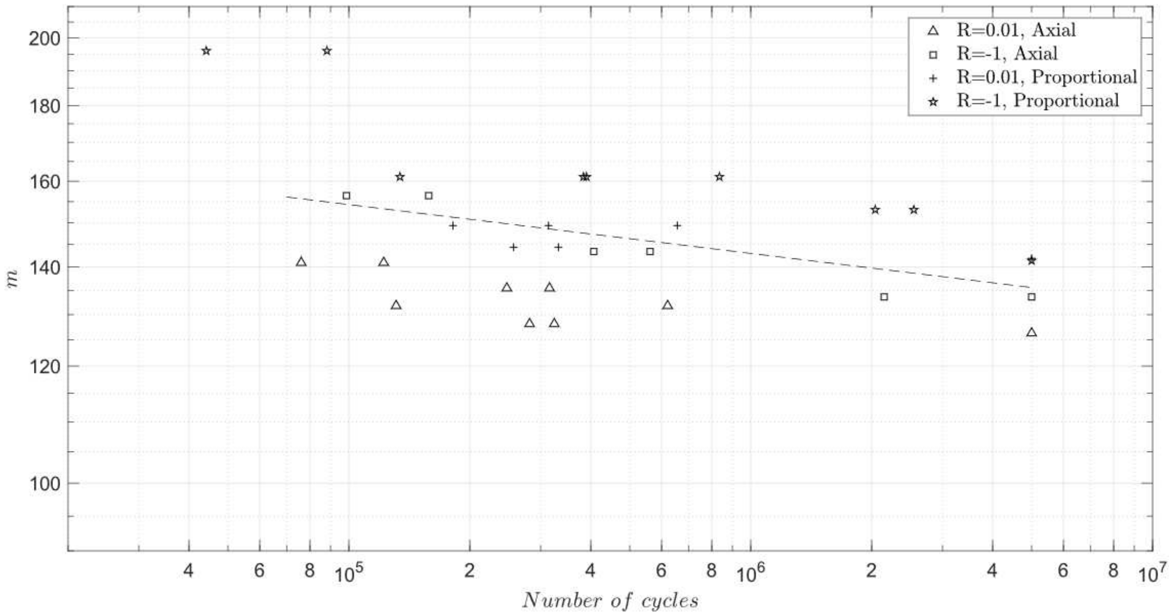

Figure 19. McDiarmid damage parameter as function of fatigue life [42]

5.2.4. Dang Van

The Dang Van's multiscale approach was also combined with Basquin law, in order to estimate a fatigue curve for the S355 steel:

$$\tau_{a,max} + k_d \sigma_{h,max} = \tau_f'(2N_f)^B \,, \tag{41}$$

where, k_d is a constant which was determined through three different methods, in order to determine which of them provides the best fatigue curve for S355 steel.

Initially, the experimental axial fatigue limits determined in the experimental campaign were plotted, as can be seen in Fig. 20, and considered that k_d is equal to the slope of the linear regression applied to these points. Thus, accordingly to this method proposed in [20], k_d=*0.367*.

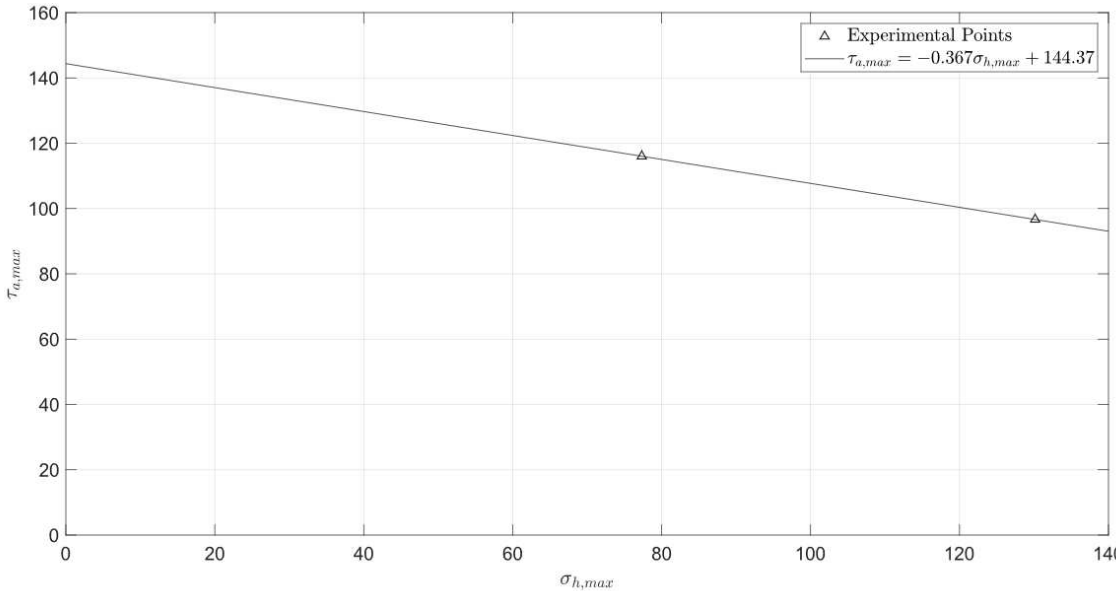

Figure 20. Axial fatigue limits for R=0 and R=-1 (see Table 7) plotted and respective linear regression [42]

The fatigue curve equation (Eq. 42) and graph (Fig. 21) achieved to k_d=*0.367* were the following ones:

$$\begin{cases} d = 253.93\, N_f^{-0.035} \\ R^2 = 0.319 \end{cases}, \tag{42}$$

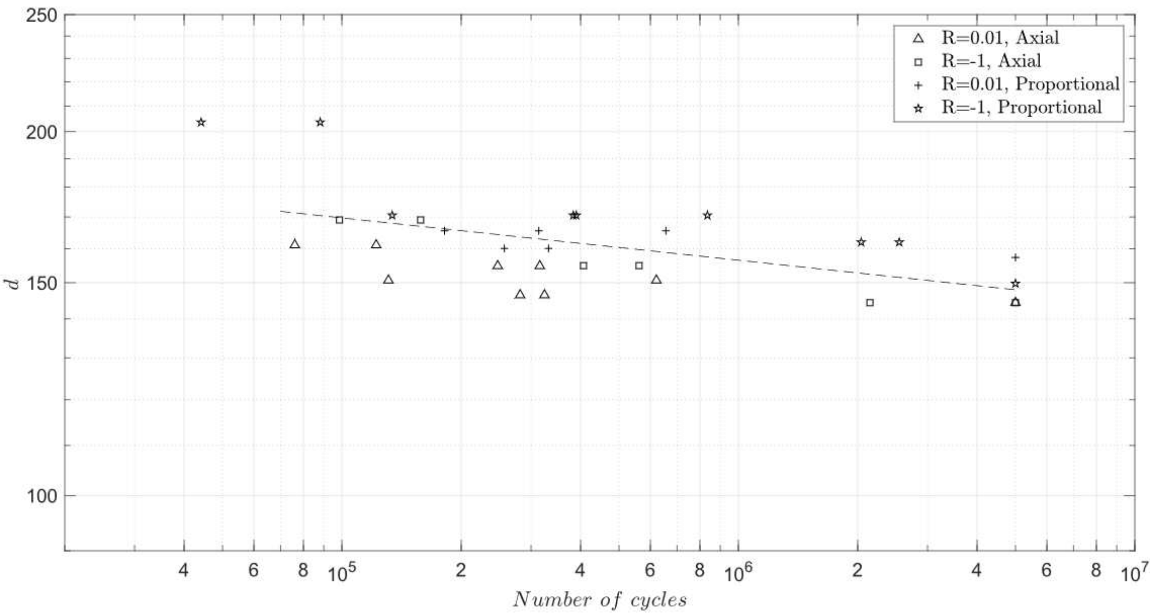

Figure 21. Dang Van damage parameter as function of fatigue life for $k_d = 0.367$ [42]

Afterwards, the same approach proposed by the authors in Section 5.1.1 can be followed to estimate the Dang Van parameter, k_d, where all fatigue limits available from the fatigue tests under uniaxial and multiaxial loading conditions for all stress ratios (R) under consideration are used. Thus, a linear regression analysis based on the two-parameter log-normal distribution can again be conducted to obtain the k_d parameter [44]:

$$\tau_{a,max,i} = (k_d) \cdot \sigma_{h,max,i} - \tau_{a,max,0}, \tag{43}$$

$$\tau_{a,max,0} = \bar{\tau}_{a,max} + (k_d) \cdot \bar{\sigma}_{h,max}, \tag{44}$$

$$-k_d = \frac{\sum_{i=1}^{n}\left(\sigma_{h,max,i} - \bar{\sigma}_{h,max}\right)\left(\tau_{a,max,i} - \bar{\tau}_{a,max}\right)}{\sum_{i=1}^{n}\left(\sigma_{h,max,i} - \bar{\sigma}_{h,max}\right)^2}, \tag{45}$$

where, $\tau_{a,max,i}$ is the value of a random sample and considered a dependent variable; $\sigma_{h,max,i}$ is the independent; $\tau_{a,max,0}$ is the interception with the vertical axis (value of $\tau_{a,max}$ when $\sigma_{h,max} = 0$); $\bar{\sigma}_{h,mean}$ and $\bar{\tau}_{a,oct}$ are the average values of the experimental fatigue limits of $\sigma_{h,max,i}$ and $\tau_{a,max,i}$ for several stress ratios (R) of uni- and multi-axial loading conditions, respectively; and n is the number of samples corresponding to the several stress ratios-R and loading conditions studied and considered.

Thus, the fatigue limits in $\sigma_{h,max}$ and $\tau_{a,max}$ were plotted again (Fig. 22), based on the fatigue limits for all loading conditions (axial, axial+torsional, torsional, bending, bending+torsional), which are presented in Table 7. In this way, an estimation of the Dang Van parameter is presented.

Table 7. Experimental fatigue limits in $\sigma_{h,max}$ and $\tau_{a,max}$ [42] [43]

Loading	*R*	$\sigma_{h,max}$ *MPa*	$\tau_{a,max}$ *MPa*
Axial	0.01	130	97
Axial	-1	77	116
Axial+Torsional	0.01	111	117
Axial+Torsional	-1	60	128
Torsional	-1	0	126
Torsional	-0.5	0	129
Torsional	0	0	176
Bending	0	136	102
Bending	-0.5	91	102
Bending	-1	84	127
Bending+Torsional	0	70	118
Bending+Torsional	-0.5	50	126
Bending+Torsional	-1	49	165

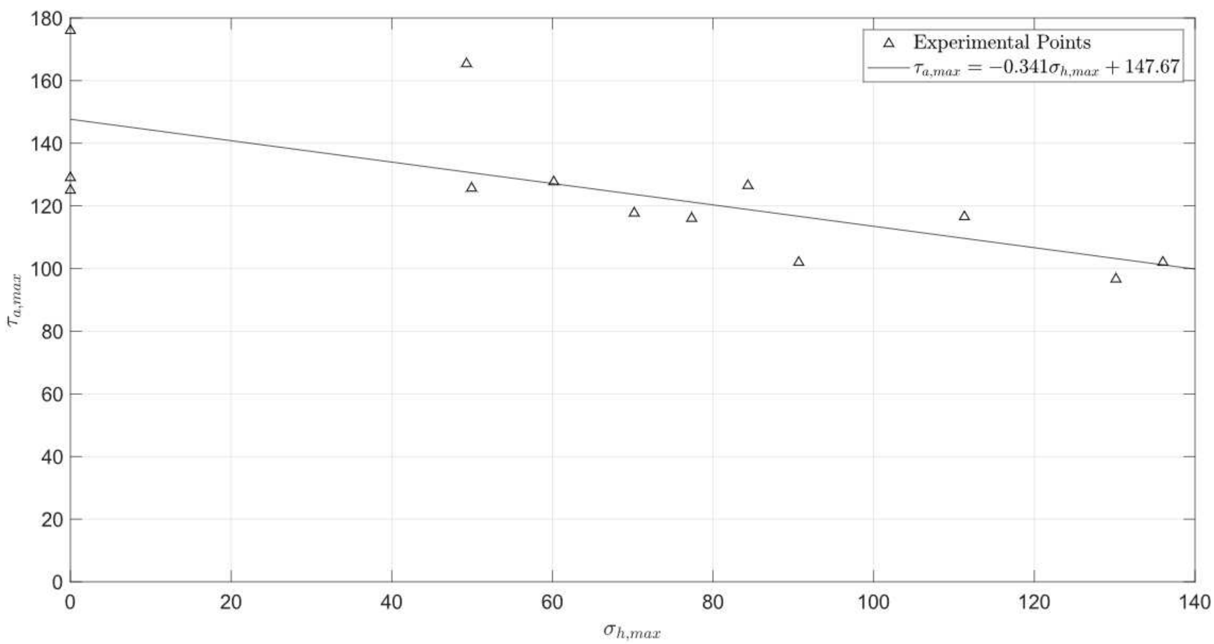

Figure 22. Fatigue limits of Table 7 plotted and respective linear regression [42]

As can be seen in Fig. 23, the slope of this linear regression is equal to 0.341. So, the mean fatigue curves were recalculated and replotted, but for k_d=*0.341* (Eq. (46)):

$$\begin{cases} d = 248.69\ N_f^{-0.035} \\ R^2 = 0.288 \end{cases}, \tag{46}$$

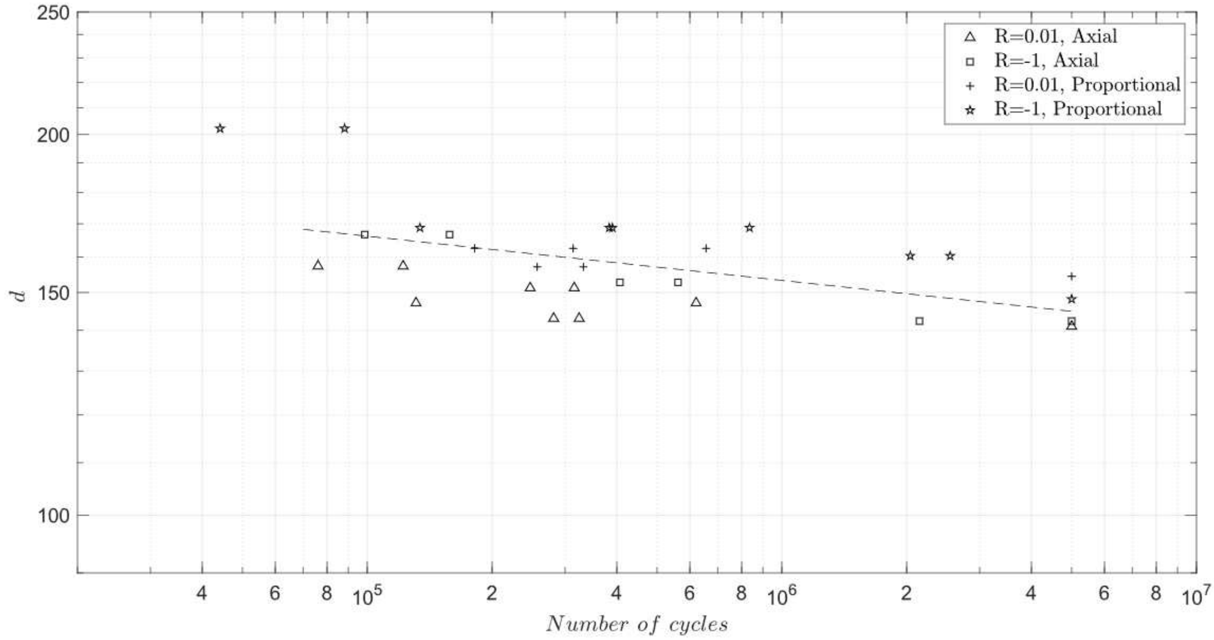

Figure 23. Dang Van damage parameter as function of fatigue life for $k_d = 0.341$ [42]

Lastly, the value of k_d was calculated through the application of Eq. (13) proposed by Dang Van and Maitournam [21]. Subsequently, the mean fatigue curves using Dang Van's model were calculated with k_d=*0.587* (Fig. 24 and Eq. (47)):

$$\begin{cases} d = 297.41\ N_f^{-0.037} \\ R^2 = 0.570 \end{cases}, \tag{47}$$

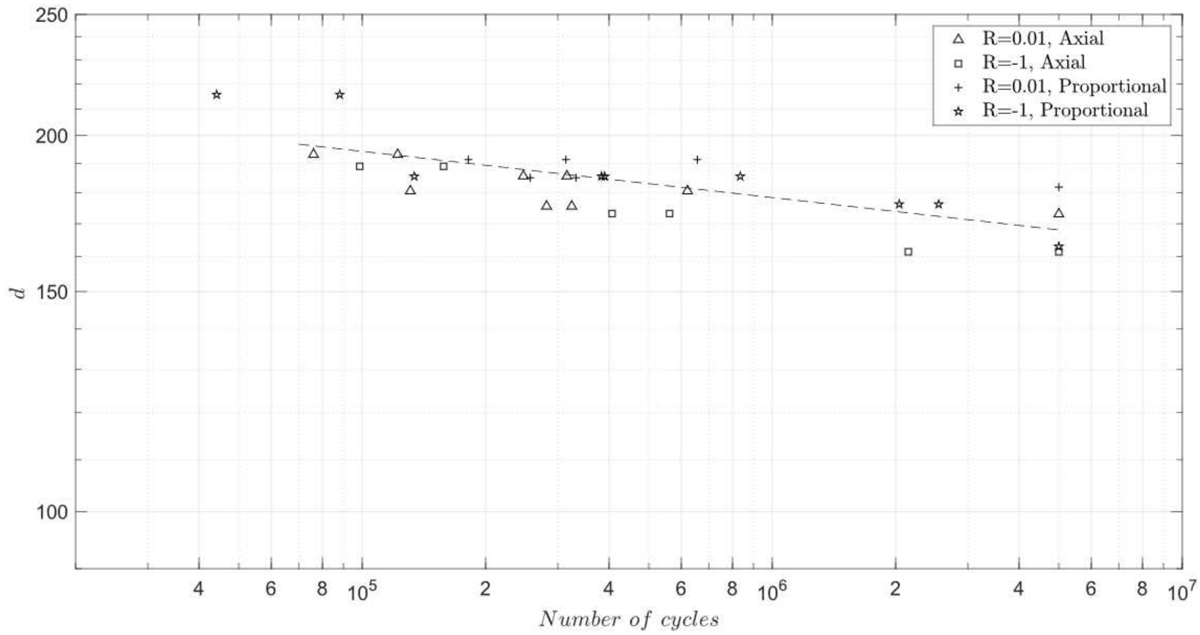

Figure 24. Dang Van damage parameter as function of fatigue life for $k_d = 0.587$ [42]

This value of k_d provides the best mean fatigue curve obtained through the application of the Dang Van's model when the coefficients of determination of the different used approaches are compared.

5.2.5. Susmel-MWCM

On the other hand, Susmel's model implies a different methodology of application to estimate fatigue life. First of all, instead of obtaining a single curve for all kinds of loading, this model establishes a design curve for each loading scenario. Thus, the design curves are defined through Eq. (48), which is the result of algebraic manipulation of Eq. (16):

$$\tau_a = \tau_{a,reff}(\rho_{eff})\left(\frac{N_f}{N_{ref}}\right)^{-\frac{1}{k_\tau(\rho_{eff})}}, \tag{48}$$

By looking at the above equation, it is concluded that there are four variables which must be determined: $\boldsymbol{\tau_{a,reff}}$, $\boldsymbol{k_\tau}$, $\boldsymbol{\rho_{eff}}$ and $\boldsymbol{N_{ref}}$. Following the procedure present on Susmel's work, $\boldsymbol{N_{ref}}$ was taken equal to $\mathbf{2 \cdot 10^6}$ cycles [40].

Then, the index *m* was calculated based on Eq. (15) and on the endurance limits of Table 8, which resulted in *m=0.31*. After that, by applying this value of *m* to Eq. (14), the different values of $\boldsymbol{\rho_{eff}}$ for each loading condition were calculated and are listed in Table 9. Regarding $\boldsymbol{\rho_{eff}}$, it is also important to determine the limit value ($\boldsymbol{\rho_{lim}}$), which was calculated through Eq. (23) as equal to 1.36.

Table 8. Fatigue limits (at $2 \cdot 10^6$ cycles) required to calculate *m* and ρ_{lim} [42], [43]

Loading Condition	*Stress parameter*	
Uniaxial, R=0.01	$\boldsymbol{\tau_a^*(MPa)}$	95
	$\boldsymbol{\sigma_{n,m}^*(MPa)}$	97
	$\boldsymbol{\sigma_{n,a}^*(MPa)}$	95
Uniaxial, R=-1	$\boldsymbol{\sigma_a(MPa)}$	232
Torsional, R=-1	$\boldsymbol{\tau_a(MPa)}$	183

The next step was to calibrate this model i.e., in other words, to determine constants α, , and β in Eqs. (17) and (18) through the values for $\boldsymbol{\tau_{a,ref}}$ and $\boldsymbol{k_\tau}$ for the fully reversed uniaxial and torsional loading cases as well as the already known values for $\boldsymbol{\rho_{eff}}$, which are always 0 and 1 for these particular loading conditions, not being influenced by the value of *m* [34], [38].

Therefore, the experimental points for these loading conditions were plotted on a modified Wöhler diagram, which plots $\boldsymbol{\tau_a}$versus $\boldsymbol{N_f}$, then simple non-linear regressions were applied and subsequently $\boldsymbol{\tau_{a,ref}}$ and $\boldsymbol{k_\tau}$ were calculated. Finally, constants a, , and β were determined and the linear functions which define the values of $\boldsymbol{\tau_{a,ref}}$ and $\boldsymbol{k_\tau}$ for each value of r $\boldsymbol{\rho_{eff}}$ are defined by Eqs. (49) and (50):

$$k_\tau = 7.8\rho_{eff} + 10.4, \tag{49}$$

$$\tau_{a,ref} = -67\rho_{eff} + 183, \tag{50}$$

Subsequently, the different values of $\boldsymbol{\tau_{a,reff}}$ and $\boldsymbol{k_\tau}$ could be determined (Table 9) as well as the design curves for each loading condition.

Table 9. Values of ρ_{eff}, $\tau_{a,reff}$ and k_τ for each loading condition: (*e): are the experimental values used to calibrate this model and (*t):are the theoretical values calculated through Equations (49) and (50)

Loading Condition	$\boldsymbol{\rho_{eff}}$	$\boldsymbol{\tau_{a,reff}(\rho_{eff})}$	$\boldsymbol{k_\tau(\rho_{eff})}$
Uniaxial, R=0.01	1.32	95 (*t)	20.7 (*t)
Uniaxial, R=-1	1	116 (*e)	18.2 (*e)
Proportional, R=0.01	0.93	121 (*t)	17.7 (*t)
Proportional, R=-1	0.70	136 (*t)	15.9 (*t)
Torsional, R=-1	0	183 (*e)	10.4 (*e)

Thus, the design curves equations for uniaxial loading with R=0.01 and R=-1 are, respectively, the following ones (Eqs. (51) and (52):

$$\tau_a = 95\left(\frac{N_f}{2\cdot10^6}\right)^{-0.048}, \tag{51}$$

$$\tau_a = 116\left(\frac{N_f}{2\cdot10^6}\right)^{-0.055}, \tag{52}$$

Regarding the proportional loadings, Eqs. (53) and (54) were determined for R=0.01 and R=-1:

$$\tau_a = 121\left(\frac{N_f}{2\cdot10^6}\right)^{-0.057}, \tag{53}$$

$$\tau_a = 136\left(\frac{N_f}{2\cdot10^6}\right)^{-0.063}, \tag{54}$$

Finally, all the fatigue design curves calculated and the corresponding experimental data were plotted in a single modified Wöhler diagram and can be seen in Fig. 25.

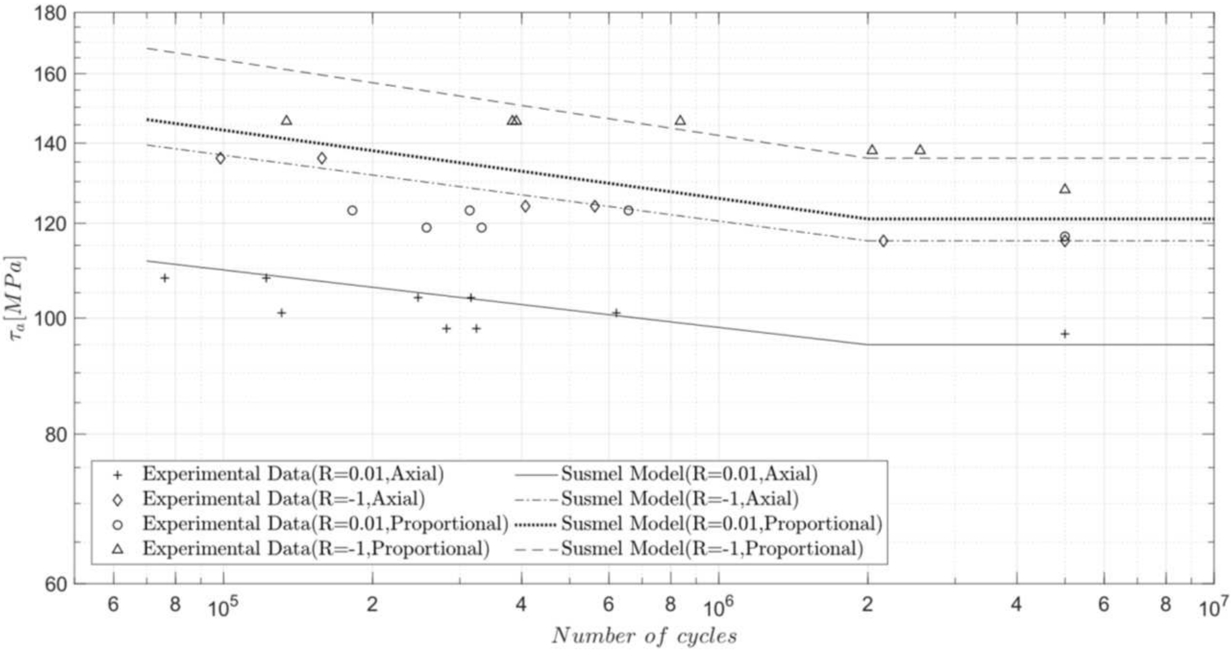

Figure 25. Fatigue design curves determined using Susmel Model for different loading conditions

As can be seen in the design curves of Fig. 25, the model under study seems to be suitable for S355 steel fatigue life estimation. The experimental points of fatigue tests are scattered around each design curve with a lower dispersion. However, for the case of proportional loading with stress ratio around zero, the model does not show such a great accordance with the experimental data. Therefore, through the fatigue data available, it is concluded that Susmel's model can be used to estimate multiaxial fatigue life of S355 steel.

5.2.6. Comparison and discussion

In this section, a comparison between different models including the approaches used to estimate their k parameters is presented. Therefore, in order to evaluate and compare the experimental models under study, three different parameters where considered and calculated: the coefficient of determination (R^2), the error index and the mean of the absolute values of the error index ($\bar{e}$).

The coefficient of determination (R^2) measures the fit quality of design curves obtained for each model to the experimental points. This variable was calculated through a Microsoft Excel inherent function [45].

Regarding the second variable mentioned, the error index, it portrays the deviation between the estimated fatigue damage and the experimental fatigue damage observed at a certain number of cycles [46], [47]. This variable was calculated through Eq. (55):

$$error\ index_i\ (\%) = \frac{experimental\ value - theoretical\ value}{theoretical\ value} \cdot 100\%, i = specimen\ number, \tag{55}$$

Furthermore, it was assumed that error index calculated for each model can be defined as a random variable X_j, which follows a normal distribution with a f probability density function defined by Eq. (56):

$$f(x) = \frac{1}{\sigma\sqrt{2\pi}} e^{-\frac{1}{2}\left(\frac{x-\mu}{\sigma}\right)^2} [X_j \rightarrow N(\mu, \sigma^2)], j = sines, findley, mcdiarmid, dangvan, susmel, \tag{56}$$

where μ is the mean and σ is the standard deviation which characterize the normal distribution [45].

Lastly, the mean of module of error index ($\bar{e}$) was also calculated for each model with the aim of depict the relative error that is associated to fatigue life estimation proposed for each design curve calculated. This parameter is defined by Eq. (57):

$$\bar{e} = \frac{\sum_{i=1}^{n} |error\ index_i|}{n}, \tag{57}$$

where n is the number of specimens.

The three different parameters were calculated for each model's approach and are listed in Table 10. Besides, the error index values obtained for all specimens were plotted in a frequency histogram as well as the respective normal distributions for each model (Fig. 26). It is important to highlight that those graphs have two vertical axes of different scales: the left axis represents the histogram frequency and the right axis is related to the *f* probability density function which is also portrayed in the graph.

Table 10. Summary table of models studied.

Models		*k* parameter	R^2	Error index (%)		$\bar{e}$ (%)
				μ	σ	
Sines	Sines [8], [9]	0.095	0.349	-0.20	6.78	5.2
	Proposed approach (Fig. 11 and Eqs. (28) to (30))	0.122	0.451	0.64	5.85	4.4
Findley	Eq. (6) according to ref. [32]	0.425	0.359	0.00	7.58	6.4
	Eq. (7) according to ref. [32]	0.228	0.378	0.35	6.50	5.1
	Eq. (8) according to ref. [32]	0.192	0.296	0.68	7.57	6.0
	Proposed approach (Fig. 17)	0.304	0.466	-0.09	5.65	4.5
McDiarmid	McDiarmid [17], [33]	0.152	0.173	0.39	9.90	7.8
Dang Van	Lieshout et al. [18]	0.367	0.319	0.15	6.99	5.5
	Proposed approach (Fig. 23 and Eqs. (43) to (45))	0.341	0.288	0.62	7.49	5.8
	Dang Van and Maitournam [21]	0.587	0.570	-0.31	4.35	3.4
Susmel	Susmel [27], [34]–[36], [38], [40]	-	-	-3.25	4.45	4.0

According to R^2 and $\bar{e}$, the best approach is the one proposed by Dang Van considering a *k* parameter equal to 0.587 as proposed by Dang Van and Maitournam [21]. Nevertheless, the Susmel's model also shows a mean of absolute errors reasonable low and close to the value obtained through Dang Van's model. However, it is important to highlight that Susmel's model requires more parameters and information to define the design curves than the other models.

Moreover, the proposed approaches to Sines' and Findley's models also provide an estimation of fatigue behaviour and damage of great accuracy and low error index, which absolute mean is above 5%.

On the other hand, McDiarmid's model seems to conduct to high values of absolute and not absolute errors index mean as well as a low capacity of adjustment of mean curve as it is portrayed in the value of R^2.

The observations and conclusions described above are enhanced by the frequency histograms of Fig. 26, where can be observed not only the error index values but also their distribution and dispersion. As expected, both Dang Van's model (with k_d =0.587) and Susmel's model show low error index values, mainly located around zero and with a low dispersion. Additionally, it is, once again, clear the inability of McDiarmid's model to describe fatigue behaviour of S355 steel since it achieves error index values close do 30%.

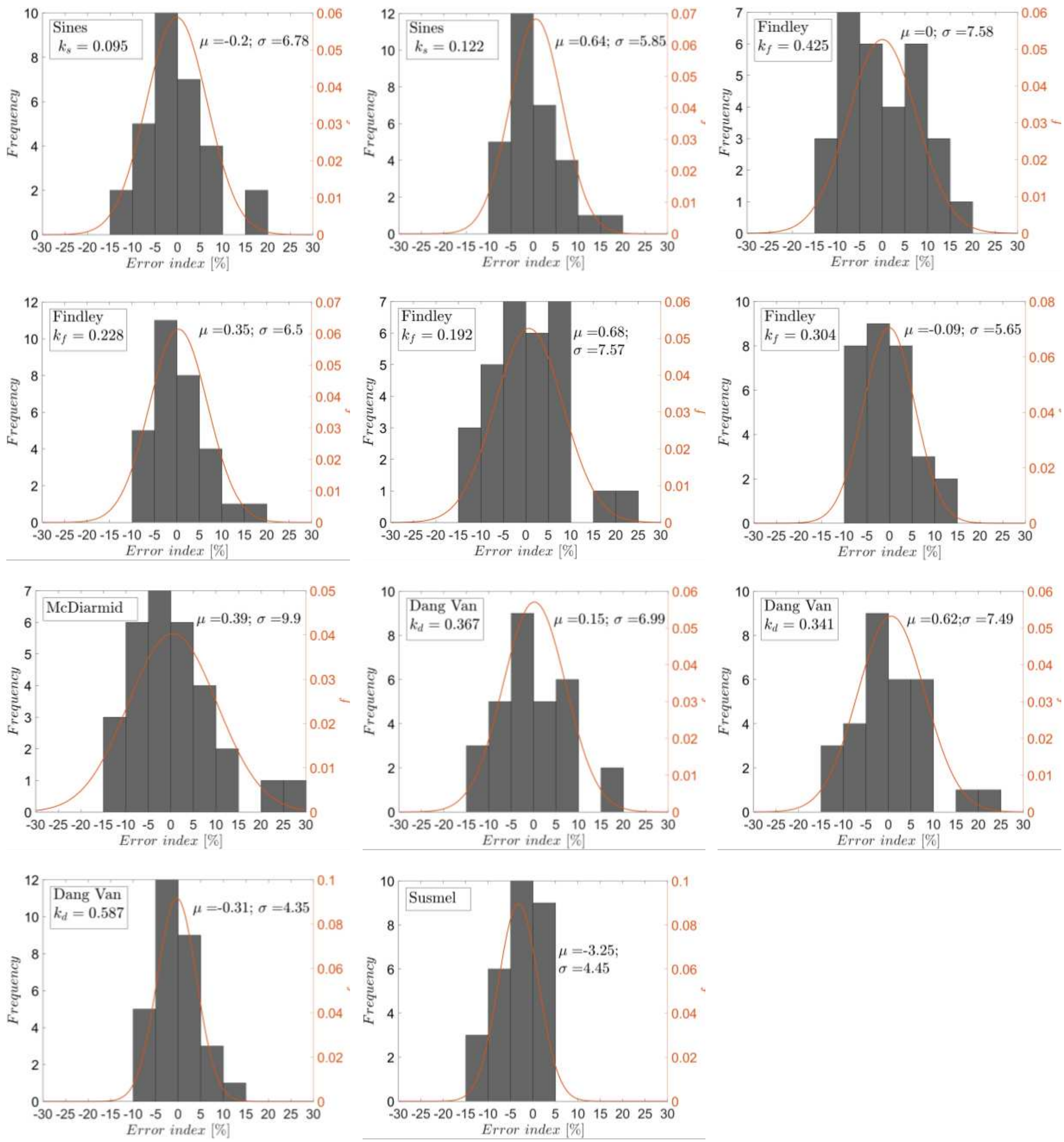

Figure 26. Frequency histograms and density functions of the normal distribution of the error index plotted for each model.

In sum, regarding the results presented by the application of the Sines' model, the most appropriate approach for estimating the k parameter was the approach proposed in this paper, which takes into account all available fatigue limits coming from different loading conditions, according to Table 4 and Fig. 11. The same happens when analysing the results of the approaches used to calculate the k parameter of the Findley's model: the approach proposed in this research work, according to Table 6 and Fig. 17, leads to the best criterion for obtaining the Findley mean fatigue curve. Moreover, in this investigation, the McDiarmid's model proved to be the most inadequate for analysing experimental fatigue results of the S355 steel under axial and multiaxial loading conditions. Last of all, the Dang Van's model for $k_d = 0.587$ and the Susmel's model appear to be the most suitable to describe S355 steel fatigue behaviour in high cycle region, but the last one requires more parameters and effort to define it.

In Fig. 27 (a) and (b), the experimental number of cycles obtained in each fatigue test is compared with the Dang Van's and Susmel's number of cycles calculated for each experimental test through the mean fatigue curves estimated. As expected, almost all points are placed between lines of multiplicity five and a great number of them are between lines of multiplicity two.

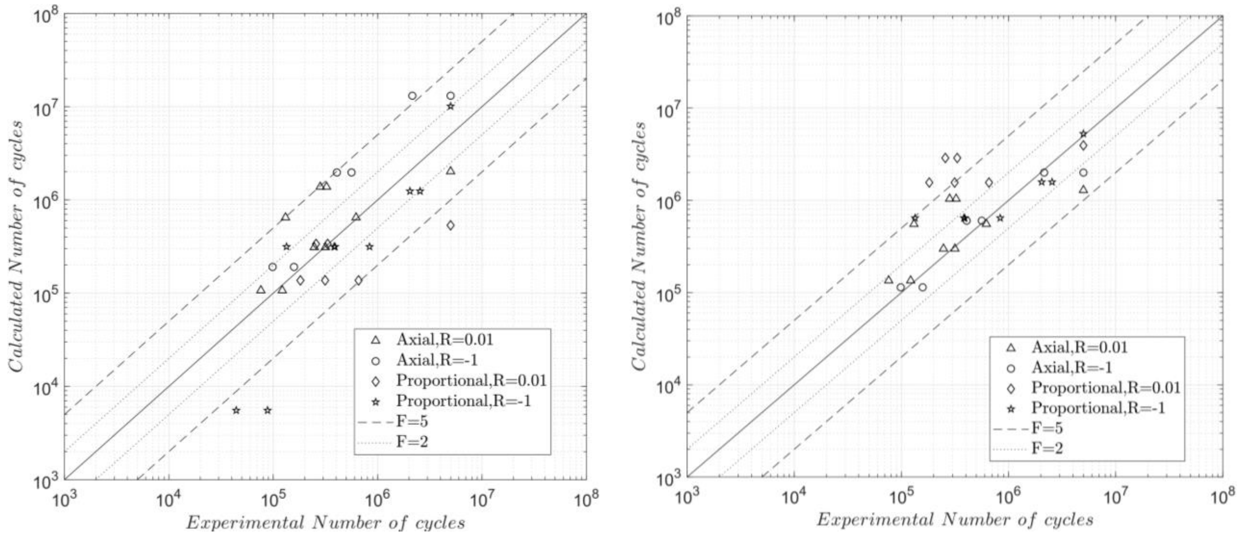

(a) (b)

Figure 27. Calculated number of cycles versus experimental number of cycles until failure graph for: (a) Dang Van's model (k_d=0.587) and (b) Susmel's model [42]

6. CONCLUSIONS

Throughout this work, axial and proportional (axial and torsional) fatigue tests were performed in S355 steel under stress ratio equal to 0 and -1 for the high-cycle region. The experimental data obtained were analysed and studied aiming at evaluating five different multiaxial fatigue models which were also explained and discussed. Therefore, axial S-N curves for two different stress ratios were determined (R=-1 and R=0) as well as calculated mean fatigue curves for axial and proportional experimental fatigue data, considering different models and constants.

Subsequently, it was concluded that the McDiarmid's model should not be considered to evaluate fatigue behaviour of S355 steel, while the models proposed by Findley and Sines, considering the proposed *k* parameters, are acceptable choices to assess it. However, Dang Van's and Susmel's models provided the best mean fatigue curves to represent S355 steel in terms of high cycle fatigue in case of a proportional loading.

In the future research work, a probabilistic analysis should be conducted, and a probabilistic design curve obtained to complete this study.

CRediT authorship contribution statement

Rita Dantas: execution of experimental tests, data analysis, writing. José Correia: data analysis, writing, validation, supervision. Grzegorz Lesiuk: execution of experimental tests, data analysis, supervision. Dariusz Rozumek: Data analysis, writing, validation. Shun-Peng Zhu: data analysis, supervision, writing - review. Abílio De Jesus: data analysis, supervision, writing - review. Luca Susmel: data analysis, supervision, writing - review. Filippo Berto: data analysis, supervision, writing - review.

ACKNOWLEDGEMENTS

This work was financially supported by base funding - UIDB/04708/2020 and programmatic funding - UIDP/04708/2020 of the CONSTRUCT - Instituto de I&D em Estruturas e Construções - funded by national funds through the FCT/MCTES (PIDDAC). This research was also funded by grant number POCI-01-0145-FEDER-030103 FiberBridge—Fatigue strengthening and assessment of railway metallic bridges using fiber-reinforced polymers by FEDER funds through COMPETE2020 (POCI) and by national funds (PIDDAC) through the Portuguese Science Foundation (FCT/MCTES). Additionally, the authors would like to thank the experimental program support given by Wroclaw University Science and Technology and Opole University of Technology (Poland).

REFERENCES

[1] M. Kamal and M. M. Rahman, "Advances in fatigue life modeling: A review," *Renew. Sustain. Energy Rev.*, vol. 82, pp. 940–949, 2018.

[2] ASTM International, "ASTM 1823-13:Standard Terminology Relating to Fatigue and Fracture," in *Annual book of ASTM standards*, West Conshohocken, PA, 2013, pp. 1–25.

[3] W. Schütz, "A History of Fatigue," *Eng. Fract. Mech.*, vol. 54, no. 2, pp. 263–300, 1996.

[4] A. R. Kallmeyer, A. Krgo, and P. Kurath, "Evaluation of HCF Multiaxial Fatigue Life Prediction Methodologies for Ti-6Al-4V," *J. Eng. Mater. Technol.*, vol. 124, no. 2, pp. 1–12, 2002.

[5] Y. Lee, M. E. Barkey, and H.-T. Kang, *Metal Fatigue Analysis Handbook- Pratical Problem-Solving Techniques for Computer Aided Engineering*. Elsevier, 2012.

[6] H. J. Gough and H. V Pollard, "The Strength of Metals under Combined Alternating Stresses," *Proc. Inst. Mech. Eng.*, vol. 131, no. (3), pp. 3–103, 1935.

[7] W. N. Findley, *A theory for the effect of mean stress on fatigue of metals under combined torsion and axial load or bending*. Engineering Materials Research Laboratory, Division of Engineering,Brown University, 1958.

[8] G. Sines, "Failure of materials under combined repeated stresses with superimposed static stresses," *Natl. Advis. Comm. Aeronaut.*, 1955.

[9] G. Sines, "Behavior of Metals under Complex Static and Alternating Stresses," in

Metal Fatigue, J. L. Sines, G. and Waisman, Ed. McGraw-Hill, 1959, pp. 145–169.

[10] T. Matake, “An Explanation on Fatigue Limit under Combined Stress,” *Bull. JSME*, vol. 20, no. 141, pp. 257–263, 1977.

[11] S. Sadek and M. Olsson, “A probabilistic method for multiaxial HCF based on highly loaded regions below the threshold depth,” *Int. J. Fatigue*, vol. 87, pp. 91–101, 2016.

[12] A. Fatemi and N. Shamsaei, “Multiaxial fatigue : An overview and some approximation models for life estimation,” *Int. J. Fatigue*, vol. 33, no. 8, pp. 948–958, 2011.

[13] M. W. Brown and K. J. Miller, “A Theory for Fatigue Failure Analysis under Multiaxial Stress-Strain Conditions,” *Appl. Mech. Gr.*, vol. 187, no. 65/73, pp. 745–755, 1973.

[14] R. I. Stephens, A. Fatemi, R. R. Stephens, and H. O. Fuchs, *Metal Fatigue in Engineering*, Second. John Wiley & Sons, Inc., 2001.

[15] K. N. Smith, P. Watson, and T. H. Topper, “A stress – strain function for the fatigue of metals,” *J. Mater.*, vol. 5, no. 4, pp. 767–778, 1970.

[16] A. L. I. Fatemi and F. Socie, “A Critical Plane Approach to Multiaxial Fatigue Damage Including Out-of-Phase Loading,” *Fatigue Fract. Eng. Mater. Struct.*, vol. 1, no. 3, pp. 149–165, 1988.

[17] D. L. McDiarmid, “A general criterion for high cycle multiaxial fatigue failure,” *Fatigue Fract. Eng. Mater. Struct. Ltd*, vol. 14, no. 4, 1991.

[18] S.-B. Lee, “Out-of-Phase, Combined Bending and Torsion Fatigue of Steels,” in *Biaxial and Multiaxial Fatigue*, M. W. Brown and K. J. Miller, Eds. London: Mechanical Engineering Publications, 1989, pp. 621–634.

[19] K. Dang-van, “Macro-Micro Approach in High-Cycle Multiaxial Fatigue,” in *Advances in MultiaxialFatigue*, D. L. McDowell and R. Ellis, Eds. Philadelphia: American Society for Testing and Materials, 1993, pp. 120–130.

[20] P. S. Van Lieshout, J. H. Den Besten, M. L. Kaminski, P. S. Van Lieshout, and J. H. Den Besten, “Validation of the corrected Dang Van multiaxial fatigue criterion applied to turret bearings of FPSO offloading buoys Validation of the corrected Dang Van multiaxial fatigue criterion applied to turret bearings of FPSO offloading buoys,” *Ships Offshore Struct.*, vol. 12, no. 4, pp. 521–529, 2017.

[21] K. Dang Van and M. H. Maitournam, “Rolling contact in railways : modelling , simulation and damage prediction,” *Fatigue Fract Engng Mater Struct*, vol. 26, pp. 939–948, 2003.

[22] H. Desimone, A. Bernasconi, and S. Beretta, “On the application of Dang Van criterion to rolling contact fatigue,” *Wear*, vol. 260, no. February, pp. 567–572, 2006.

[23] A. Callens and A. Bignonnet, “Fatigue design of welded bicycle frames using a multiaxial criterion,” *Procedia Eng.*, vol. 34, pp. 640–645, 2015.

[24] I. V. Papadopoulos, “A new criterion of fatigue strength for out-of- phase bending and torsion of hard metals,” *Fatigue*, vol. 16, pp. 377–384, 1994.

[25] A. Carpinteri and A. Spagnoli, “Multiaxial high-cycle fatigue criterion for hard metals,” *Int. J. Fatigue*, vol. 1, pp. 135–145, 2001.

[26] A. Carpinteri, C. Ronchei, D. Scorza, and S. Vantadori, “Critical Plane Orientation Influence on Multiaxial High-Cycle Fatigue Assessment,” *Phys. Mesomech.*, vol. 18, no. 4, pp. 348–354, 2015.

[27] L. Susmel and R. Tovo, “Estimating fatigue damage under variable amplitude multiaxial fatigue loading,” *Fatigue Fract. Eng. Mater. Struct.*, vol. 34, pp. 1053–1077, 2011.

[28] Y. Liu and S. Mahadevan, “Multiaxial high-cycle fatigue criterion and life prediction for metals,” *Int. J. Fatigue*, vol. 27, pp. 790–800, 2005.

[29] J. Schijve, *Fatigue of Structures and Materials*. United States of America: Kluwer

Academic Publishers, 2001.

[30] D. Socie, “Critical plane approaches for multiaxial fatigue damage assessment,” in *DTP1191-EB Advances in Multiaxial Fatigue*, D. McDowell and R. Ellis, Eds. West Conshohocken, PA: ASTM International, 1993, pp. 7–36.

[31] D. McDowell and J. Ellis, “Overview,” in *Advances in Multiaxial Fatigue*, D. McDowell and J. Ellis, Eds. West Conshohocken, PA: ASTM International, 1994, pp. 1–4.

[32] D. Socie, “Multiaxial stress-life technical background,” 2018. [Online]. Available: https://www.efatigue.com/multiaxial/background/stresslife.html.

[33] L. McDiarmid, “A shear stress based critical-plane criterion of multiaxial fatigue failure for design and life prediction,” *Fatigue Fract. Eng. Mater. Struct. Ltd*, vol. 17, no. 12, pp. 1475–1484, 1995.

[34] L. Susmel and P. Lazzarin, “A bi-parametric Wöhler curve for high cycle multiaxial fatigue,” *Fatigue Fract. Eng. Mater. Struct.*, vol. 25, pp. 63–78, 2002.

[35] L. Susmel, “Multiaxial fatigue limits and material sensitivity to non-zero mean,” *Fatigue Fract. Eng. Mater. Struct.*, vol. 31, pp. 295–309, 2008.

[36] L. Susmel, D. G. Hattingh, M. N. James, and R. Tovo, “Multiaxial fatigue assessment of friction stir welded tubular joints of Al 6082-T6,” *Int. J. Fatigue*, vol. 101, pp. 282–296, 2017.

[37] L. Susmel and R. Tovo, “Estimating fatigue damage under variable amplitude multiaxial,” *Fatigue Fract. Eng. Mater. Struct.*, vol. 34, pp. 1053–1077, 2011.

[38] L. Susmel, “On the estimation of the material fatigue properties required to perform the multiaxial fatigue assessment,” *Fatigue Fract. Eng. Mater. Struct.*, vol. 36, pp. 565–585, 2013.

[39] L. Susmel, “A simple and efficient numerical algorithm to determine the orientation of the critical plane in multiaxial fatigue problems,” *Int. J. Fatigue*, vol. 32, no. 11, pp. 1875–1883, 2010.

[40] L. Susmel, *Multiaxial notch fatigue: From nominal local stress/strain quantities*. Woodhead Publishing Limited, 2009.

[41] J. A. F. O. Correia, A. M. P. de Jesus, A. Fernández-Canteli, and R. A. B. Calçada, “Modelling probabilistic fatigue crack propagation rates for a mild structural steel,” *Frat. ed Integrita Strutt.*, vol. 31, pp. 80–96, 2015.

[42] R. Dantas, “Fatigue life estimation of steel half-pipes bolted connections for onshore wind towers applications,” University of Porto, 2019.

[43] D. Rozumek and R. Pawliczek, *Opis rozwoju pęknięć i zmęczenia materiałów w ujęciu energetycznym. Wieloosiowe zmęczenie losowe elementów maszyn i konstrukcji cz. VII*. Opole: Wydawnictwo Politechniki Opolskiej, 2004.

[44] ASTM International, *E 739 – 91: Standard Practice for Statistical Analysis of Linear or Linearized Stress-Life (S-N) and Strain-Life (e -N) Fatigue Data*, vol. 91. West Conshohocken, PA, 2004.

[45] R. C. Guimarães and J. A. S. Cabral, *Estatística*. Alfragide: McGraw-Hill, 1997.

[46] I. V. Papadopoulos, P. Davoli, C. Gorla, M. Filippini, and A. Bernasconi, “A comparative study of multiaxial high-cycle fatigue criteria for metals,” *Int. J. Fatigue*, vol. 19, no. 3, pp. 219–235, 1997.

[47] J. Zhang, D. Shang, Y. Sun, and X. Wang, “Multiaxial high-cycle fatigue life prediction model based on the critical plane approach considering mean stress effects,” *Int. J. Damage Mech.*, vol. 27, no. 1, pp. 32–46, 2018.